MET.O.11 TECHNICAL NOTE NO.86

RECENT DEVELOPMENTS OF THE NON HYDROSTATIC MESOSCALE MODEL

by

K M CARPENTER and M C TAPP

JUNE 1977.

MET O 11 TECHNICAL NOTE No.86

RECENT DEVELOPMENTS OF THE NON HYDROSTATIC MESOSCALE MODEL

by

K M Carpenter and M C Tapp

SUMMARY

In the last few years the mesoscale model has been developed in three ways: the study of orographic effects, sea breezes in real situations and convective storms. There have also been some changes to the basic model.

The major technical advance has been in the solution of the Helmholtz equations that result from the treatment of sound waves by implicit finite difference methods. Formerly, an Alternating Direction Implicit (ADI) iterative method was used, but a direct method of solution is now used and is superior to the ADI method in all respects. The specification of boundary conditions remains a problem, the most important difficulty being the failure to guarantee the outward propagation of wave energy. Methods of removing grid-scale roughness without using excessive diffusion are also being investigated.

Orography has been included in the model by using model levels that follow the surface exactly. A series of simulations of flow past an isolated hill is being carried out.

14 June 1973 was selected as "a good sea breeze day" over England and Wales, and a model forecast has been made for that day. On this occasion the interesting features were driven by surface heating so a detailed surface exchange scheme was used and appeared satisfactory in spite of the difficulty of choosing realistic representative values for some of the parameters involved. The description of boundary layer turbulence requires further development and only gives good boundary layer profiles for potential temperature during the day. More generally the results are encouraging, particularly if the imposition of a static synoptic situation is allowed for.

A simple study of cumulus convection was undertaken using the same data as Bennetts (1977). Initially, the object was to test the model in a different format to that required for sea breeze studies, and to provide a context for the

inclusion of the hydrological cycle. The results are presented in the text and confirm the suitability of the model for simulating convection. In this version of the model, it was found to be expedient to change the finite difference calculation of the advection of water variables from the usual centred differences to a quasi Lagrangion method.

1 INTRODUCTION

The basic formulation of a non-hydrostatic mesoscale model has already been described in two papers by Tapp and White (1974, 1976). This paper summarises the progress made in the past three years.

The mesoscale model was developed to study the detailed structure and local modifications of mesoscale weather systems. In order to simulate a wide range of systems the model was designed to be as flexible as possible, and it is now proving to be a very versatile tool. Three areas of progress have emerged: the study of orographic effects (lee waves), sea breezes and convective storms. This has produced three versions of the model each containing parameterisations of the physical processes that are believed to be important in the system being studied, but the models have a common organisation and basic formulation.

For most synoptic meteorologists the novel feature of the model is that the hydrostatic approximation is not made; other assumptions such as the anelastic or incompressibility approximations are also avoided. This approach has been justified in the first report and is, for some of the scales studied, clearly necessary. It is also desirable, since the three dimensional structure of the equations simplifies the interpretation of model results. One might expect that the inclusion of sound waves in the basic equations involves a substantial computational penalty, but this is not the case. If the Met Office (hydrostatic) operational forecast model were run with a 10 km grid it would require a time step of about 90 secs or less. The time step used for the mesoscale model is usually 60 secs, but it could be increased up to 100 secs (independent of grid length) in most conditions. Thus the computer time requirements of the mesoscale model and a hydrostatic model are comparable for a grid length of 10 km.

In Section 2 developments in the basic model formulation are described. This includes a new method of solving the Helmholtz equations that arise from the implicit treatment of sound waves. The method of determining lateral and upper boundary values has been changed, but this is more conveniently discussed in the later sections.

Section 3 is a description of the inclusion of orography. In order to test the model, a series of integrations in simple idealised conditions is being carried out and some of these will eventually be compared with analytical results.

The application of the model to sea breezes, in particular a case study for 14 June 1973, is described in Section 4. This model is dry and the effects of orography have only recently been included, but a detailed description of surface exchanges and the turbulent boundary layer is in the model. The grid is 61 x 61 x 10 pts in a volume of 600 x 600 x 4 km^3.

The cumulus or convection model includes the effects of humidity, cloud and rain and uses a grid of 24 x 24 x 19 pts in a volume of 23 x 23 x 18 km^3. It is described in Section 5. The investigation was started in order to test the model in a completely different format to that required for sea breeze studies, and as a context for the inclusion of the hydrological cycle. These motives have been fulfilled, but the results are interesting in their own right. The initial data taken by Bennetts (1977) has been used in an attempt to simulate a cumulus cloud, and our results are summarised in Section 5.

From the wide range of applications and model formats described above it will be clear that the original aim to develop a highly flexible model has been achieved. It will emerge from the remainder of the paper that many technical problems are outstanding, but that the applications of the model are already interesting in themselves.

2 BASIC MODEL DEVELOPMENTS

Tapp and White (1974, 1976) have already described the basic model formulations in some detail. The equations they suggested, which are still used, are given in 2.1. They have now been extended in several ways as described in the later sections, but there have been a small number of changes in the way they are treated that apply to almost all the uses of the model and these are reviewed in this Section. Before the description of the new developments the basic equations are given and the notation explained.

The equations in the absence of humidity and orography are:

$$\frac{Du}{Dt} = fv - c_p(\theta_0 + \theta_1)\frac{\partial P_1}{\partial x} + F_x$$

$$\frac{Dv}{Dt} = -fu - c_p(\theta_0 + \theta_1)\frac{\partial P_1}{\partial y} + F_y$$

$$\frac{Dw}{Dt} = g\frac{\theta_1}{\theta_0} - c_p(\theta_0 + \theta_1)\frac{\partial P_1}{\partial z} + F_z$$

$$\frac{D\theta}{Dt} = Q$$

$$\frac{DP_1}{Dt} = \frac{gw}{c_p\theta_0} - (\gamma - 1)(P_0 + P_1)\left(\frac{\partial u}{\partial x} + \frac{\partial v}{\partial y} + \frac{\partial w}{\partial z}\right) + \frac{(\gamma-1)(P_0+P_1)}{(\theta_0+\theta_1)}Q \qquad 2.1$$

where $\frac{D}{Dt} = \frac{\partial}{\partial t} + u\frac{\partial}{\partial x} + v\frac{\partial}{\partial y} + w\frac{\partial}{\partial z}$

u, v, w are the components of velocity in the x, y, z directions

g, c_p, f have their usual meanings, $\gamma = c_p/c_v$

$$P = P_0 + P_1 = \left(p/p_r\right)^K \qquad 2.2$$

is the Exner function defined in terms of the pressure p, a reference pressure p_r and $K = R/c_p$ and

$$\theta = \theta_0 + \theta_1 = T/P \qquad 2.3$$

is the potential temperature.

P_0 is the value of P in a static atmosphere with constant $\theta = \theta_0$ and P_1 and θ_1 are defined in 2.2 and 2.3.

F_x, F_y and F_z represent the non-linear effects of motion that is not resolved by the grid, eg boundary layer turbulence, and any device that must be used to control grid scale roughness.

Q is the diabatic term, including processes like those represented by F.

In the finite difference representation of equation 2.1, the sound waves are controlled by an implicit time averaging scheme for part of the pressure gradient and divergence term. This allows a time step δt as large as N^{-1}, where N is the Brunt-Vaisala frequency ie the maximum frequency for gravity waves in a static atmosphere. Details of the implicit calculation are contained in Appendix 1, where the derivation of the Helmholtz equations for the normal modes $\underset{\sim}{f_i}$ of the pressure correction field π is given. With

$$\pi(t) = c_p \theta_0 \left(P_1(t+\delta t) - 2P_1(t) + P_1(t-\delta t)\right) \qquad 2.4$$

$$\nabla_H^2 \pi + \left\{ \frac{\partial^2}{\partial z^2} - \frac{g}{c_0^2} \cdot \frac{\partial}{\partial z} - \frac{1}{c_0^2 \delta t^2} \right\} \pi = G \qquad 2.5$$

where G is calculated from the current values of the model fields and the decomposition of 2.5 into normal modes of $\left\{ \frac{\partial^2}{\partial z^2} - \frac{g}{c_0^2} \frac{\partial}{\partial z} - \frac{1}{c_0^2 \delta t^2} \right\}$ gives

$$\nabla_H^2 f_i - \lambda_i f_i = \beta_i \qquad 2.6$$

where the suffix i label the normal mode with eigenvalue λ_i.

Details of the above can be found in Tapp and White (1974, 1976). More recent developments are now described.

i. Convective adjustment.

Early integrations of equations 2.1 did not include any convective adjustment and, when a sea breeze was driven by surface heating, a very regular pattern of grid scale convection was set up. There were also a few isolated storms where differential advection had produced static instability. This behaviour did not appear to damage the other model results, but it is the usual practice to include convective adjustment procedures in numerical atmospheric models and this has now been done for the mesoscale model.

Lapse rate instability is controlled by mutually adjusting adjacent layers so as to remove a proportion of the instability. Parameters can be tuned so that the lapse rate is brought to a chosen slightly stable value over a chosen period of time.

ii. Time filter.

A time filter of the form

$$\chi^{*(n+1)} = \chi^{(n-1)} + 2\delta t \left(\frac{\partial \chi}{\partial t}\right)^{(n)}$$

$$\chi^{(n)} = (1-2\mu)\chi^{*(n)} + \mu\left(\chi^{(n-1)} + \chi^{*(n+1)}\right) \qquad 2.7$$

has been introduced with

$$\mu = 0.02$$

This value of μ effectively controls time level separation and damps the $4\delta t$ oscillations noted by Tapp and White (1974).

iii. Diffusion.

Various forms of non-linear and non-isotropic diffusion have been tested in the model. With the present finite difference approximations, the group velocity of two grid length waves vanishes and roughnesses tend to accumulate. This is a well-known problem and a variety of solutions is available. A novel approach, which is currently being tested, is to use a non-linear, non-isotropic diffusion of the sort given in 2.8

$$\left(\frac{\partial \chi}{\partial t}\right)_{diffusion} = K\left(\frac{\partial^2 \chi}{\partial x^2}\right)_3 \left[\left(\frac{\partial^2 \chi}{\partial x^2}\right)_3 \Big/ \left\{\left(\frac{\partial^2 \chi}{\partial x^2}\right)_5 + \frac{8K\delta t}{\delta x^2}\left(\frac{\partial^2 \chi}{\partial x^2}\right)_3\right\}\right]$$

$$+ K\left(\frac{\partial^2 \chi}{\partial y^2}\right)_3 \left[\left(\frac{\partial^2 \chi}{\partial y^2}\right)_3 \Big/ \left\{\left(\frac{\partial^2 \chi}{\partial y^2}\right)_5 + \frac{8K\delta t}{\delta y^2}\left(\frac{\partial^2 \chi}{\partial y^2}\right)_3\right\}\right]$$

$$+ Z \text{ term.} \qquad 2.8$$

where

$$\left(\frac{\partial^2 \chi}{\partial x^2}\right)_3 = \frac{\chi_{K+1} - 2\chi_K + \chi_{K-1}}{\delta x^2}$$

is the usual way, and

$$\left(\frac{\partial^2 \chi}{\partial x^2}\right)_5 = \frac{\chi_{K+2} - 2\chi_K + \chi_{K-1}}{4\delta x^2}$$

This form of diffusion has the advantage that, for most scales of motion,

$$\left(\frac{\partial^2 \chi}{\partial x^2}\right)_6 \approx \left(\frac{\partial^2 \chi}{\partial x^2}\right)_3$$

and

$$\left(\frac{\partial \chi}{\partial t}\right)_{diffusion} \approx \frac{K}{1 + \frac{8K\delta t}{\delta x^2}}\left(\frac{\partial^2 \chi}{\partial x^2} + \frac{\partial^2 \chi}{\partial y^2} + \frac{\partial^2 \chi}{\partial z^2}\right)$$

so that the value of the diffusion coefficient can be chosen with some degree of physical insight. However, for two grid length waves

$$\left(\frac{\partial^2 \chi}{\partial x^2}\right)_5 = 0$$

so that

$$\left(\frac{\partial \chi}{\partial t}\right)_{diffusion} = \frac{\delta x^2}{8\delta t} \frac{\partial^2 \chi}{\partial x^2} + \text{other terms.}$$

which completely removes a two grid length wave in a single application.

iv. Boundary Conditions

Several problems have arisen in the use of the lateral and upper boundary conditions suggested by Tapp and White (1974). This is more conveniently discussed in later sections since the nature and solution of the problems has varied according to the application. No attempt has been made to vary the imposed boundary values during an integration, but this will be done shortly as described in Section 4.

v. Solution of Helmholtz equations

Until recently the Helmholtz equations 2.6 were solved by Alternating Direction Implicit (ADI) iterative methods, which were considered very efficient. However, this has two disadvantages. The first is that the entire r.h.s. field must be held in core until the equation is solved, and then the solutions must be held in core until they can be used to complete the calculations of the model fields at the future time; this is wasteful of main storage. The second is that the ADI method fails to converge when the horizontal grid of the model is decreased and the depth of the model is increased; this is explained in Appendix I.

Tapp (1976) has developed a direct method of solving 2.6 using known theory, and the new technique is described in Appendix I. It is based on a normal mode decomposition in one direction (the x direction), which in practice takes the form of a Fast Fourier Transform, followed by a double sweep Gaussian elimination in the other direction (the y direction).

In terms of computing time, it has been found that the direct method is comparable with a small number of ADI iterations so there has been a small gain in that respect. The fact that the direct solution works on a row of data as opposed to the whole two dimensional field means that the storage requirements are reduced. In the case of the convective model the saving in core is about 20% or 90K bytes. The final advantage of the direct method of solving the Helmholtz equations is that it works where the ADI method failed.

3. OROGRAPHY

Two principles guided the choice of method for introducing the effects of orography into the model. The first was that the model equations should remain as simple as possible, and the second was that the methods of integrating the equations should be as unchanged as possible by the introduction of orography.

It was decided that the model mesh should not be embedded in the orography, as indicated by Fig. 3.1A, so that the choice was between a grid that was uniformly distorted with height (Fig. 3.1B) and a grid that was undisturbed at higher levels (eg Fig. 3.1C). Either arrangement, 1B or 1C, is achieved by a co-ordinate transformation.

$$x' = x$$

$$y' = y$$

$\eta = \eta(x,y,z)$ where $\eta(x,y,E(x,y)) = 0$ and $E(x,y)$ is the orographic height. The equations in a general (x,y,η) co-ordinate system simplify if

$$\eta = \eta(z - E(x,y)) \quad ;$$

in particular the divergence

$$\underset{\sim}{\nabla}\cdot\underset{\sim}{u} = \frac{\partial u}{\partial x} + \frac{\partial v}{\partial y} + \frac{\partial \eta}{\partial z}\cdot\frac{\partial}{\partial \eta}\left(\frac{\partial z}{\partial \eta}\right)\dot{\eta}$$

and the vertical coupling matrix for sound waves (see equation 2.5) is independent of the horizontal co-ordinates x, y. For this reason the grid shown in Fig 3.1B and the vertical co-ordinate

$$\eta = z - E(x,y) \qquad 3.1$$

were chosen.

There is a similar choice to be made in the definition of the model pressure variable, the Exner function. This can be defined by

$$P = \left(p/p_r\right)^{\kappa} \qquad 3.2$$

where p_r is a uniform pressure, or by

$$Q = \left(p/p_s\right)^{\kappa} \qquad 3.3$$

where p_s is the surface pressure in a basic atmosphere and thus a function of position, When the variables P and Q are written as the sum of a basic term given by a stationary atmosphere and a perturbation term

$$P = P_0' + P_1$$

$$Q = Q_0 + Q_1$$

the surface value of Q is relatively simple

$$P_0' = 1 - \frac{gE}{c_p \theta_0} \qquad \text{at the surface}$$

$$Q_0 = 1 \qquad \text{at the surface.}$$

so it would seem natural to choose the pressure variable Q. However, since Q depends on a basic surface pressure p_s, the horizontal pressure gradients

$$\frac{\partial P}{\partial x} = \frac{\partial}{\partial x} p_s Q^{1/\kappa} = \frac{\partial}{\partial x} p_r P^{1/\kappa}$$

are unduly complicated if written in terms of Q, so P given by 3.2 is preferred.

As indicated in the previous paragraph, P is written in terms of deviations from the value in a basic atmosphere in which

$$\theta = \theta_0$$

$$P = P_0' = 1 - \frac{g\eta}{c_p \theta_0} - \frac{gE(x,y)}{c_p \theta_0} \qquad 3.4$$

Then in general

$$\theta = \theta_0 + \theta_1$$

and

$$P = P_0 + \frac{gE}{c_p \theta_0} + P_1 \qquad 3.5$$

where $P_0 = 1 - \frac{g\eta}{c_p \theta_0}$.

3.5 is written so that P_0 is independent of x, y because the vertical coupling matrix for sound waves (see equation 2.5) involves P_0 and must be independent of x, y .

With P_1 defined by 3.2 and 3.5 and η defined by 3.1 the model equations become

$$\frac{Du}{Dt} = fv - c_p(\theta_0+\theta_1)\left(\frac{\partial P_1}{\partial x} - \frac{\partial E}{\partial x}\frac{\partial P_1}{\partial \eta}\right) = X$$

$$\frac{Dv}{Dt} = -fu - c_p(\theta_0+\theta_1)\left(\frac{\partial P_1}{\partial y} - \frac{\partial E}{\partial y}\frac{\partial P_1}{\partial \eta}\right) = Y$$

$$\frac{D\dot{\eta}}{Dt} = g\frac{\theta_1}{\theta_0} - c_p(\theta_0+\theta_1)\frac{\partial P_1}{\partial \eta} - \frac{\partial E}{\partial x}X - \frac{\partial E}{\partial y}Y$$
$$- \left\{ u^2\frac{\partial^2 E}{\partial x^2} + 2uv\frac{\partial^2 E}{\partial x\,\partial y} + v^2\frac{\partial^2 E}{\partial y^2}\right\}$$

$$\frac{DP_1}{Dt} = \frac{g}{c_p\theta_0}\left(\dot{\eta} + u\frac{\partial E}{\partial x} + v\frac{\partial E}{\partial y}\right)$$
$$-(\gamma-1)\left(P_0 - \frac{gE}{c_p\theta_0} + P_1\right)\left(\frac{\partial u}{\partial x} + \frac{\partial v}{\partial y} + \frac{\partial \dot{\eta}}{\partial \eta}\right)$$
$$+\frac{(\gamma-1)}{\theta_0+\theta_1}\left(P_0 - \frac{gE}{c_p\theta_0} + P_1\right)$$

$$\frac{D\theta_1}{Dt} = Q \qquad 3.6$$

The last term in the third momentum equation is the centrifugal acceleration in a curved co-ordinate system. Disregarding other terms, it can be written

where $$\frac{\partial \dot{\eta}}{\partial t} = -|u|^2\frac{\partial^2 E}{\partial s^2}$$

$$|u|^2 = u^2 + v^2$$

and s is horizontal distance measured in the direction of the wind. This can be shown by noting that the centrifugal acceleration along the radius of curvature is

$$\frac{\partial \dot{\eta}}{\partial t}\,\frac{1}{\sqrt{1+\left(\frac{\partial E}{\partial s}\right)^2}} = -\frac{\hat{u}^2}{R}$$

where $\hat{u}$ is velocity parallel to the surface and R is the radius of curvature.

In equation 3.6, the sound waves are treated implicitly as described in Section 2. All terms involving the orographic height E are treated explicitly, so that the equations for the implicitly treated sound waves are

$$\frac{\partial u}{\partial t} = -c_p \theta_0 \frac{\partial P_1}{\partial x}$$

$$\frac{\partial \dot{\eta}}{\partial t} = -c_p \theta_0 \frac{\partial P_1}{\partial y}$$

$$\frac{\partial P_1}{\partial t} = \frac{g\dot{\eta}}{c_p \theta_0} - (\gamma - 1) P_0 \left(\frac{\partial u}{\partial x} + \frac{\partial \dot{\eta}}{\partial \eta} \right)$$

3.7

which are identical to those in the absence of orography if η is replaced by z and $\dot{\eta}$ is replaced by ω .

The version of the mesoscale model described above is being used to study the effects of orography in two ways. Most of the sea breeze simulations have been carried out using the model without orography, but one simulation has included orography and this integration will be discussed in the next Section. The remainder of the work on orographic effects has been a series of studies of flow over an isolated hill. This series of studies is designed to test and improve the model rather than to gain an understanding of the effects of isolated hills, but the latter aspect has considerable interest.

The first experiment simulated uniform isotropic flow past an isolated hill. The results presented below can be described by the conservation of potential vorticity in the form

$$\frac{\zeta + f}{h} = \text{constant for a fluid particle}$$

3.8

where ζ is relative vorticity and

h is the depth of the model, or the atmospheric scale height. The model details are:

grid length = δx = 11 km

horizontal grid of 20 x 22 points

vertical grid of 20 levels whose spacing decreases near the ground

total depth 15.2 km

f = 6.38×10^{-4} sec^{-1} ($f = 6.38 \times 10^{-4}$ sec^{-1})

K_H = 5×10^4 m^2 sec^{-1} (interior) 1.6×10^5 m^2 sec^{-1} (boundary high diffusion zone)

K_v = 2 m^2 sec^{-1}

where K_H is the coefficient for linear, two dimensional horozontal diffusion and
K_V is the coefficient for linear, one dimensional vertical diffusion.

There are no surface exchanges of momentum or heat ie the lower boundary is a free slip, rigid, insulating, (nearly horizontal) wall. The upper and lateral boundary correlations are as described by Tapp and White (1974, 1976) except that, at the upper boundary, $\dot{\eta}$ has been calculated from the equation for horizontal flow.

ie $\omega = 0$

and all upper boundary points are treated as inflow (u specified, $\frac{\partial P}{\partial \eta}$ calculated from the momentum equations). The upstream conditions are

$$u = 10 \text{ m sec}^{-1}$$
$$\theta = \theta_0 = 298^{\circ}K$$
$$v = 0$$
$$\dot{\eta} = 0$$

The results at 3 and 6 hrs are shown in Fig. 3.2, which shows wind perturbations not total winds. The cyclonic eddy in the lee of the hill is being advected downstream by the basic flow, but the anticyclonic eddy over the hill is stationary.

The behaviour shown in Fig. 3.2 is qualitatively as expected from the conservation of potential vorticity (equation 3.8), but the induced relative vorticity is too small. Changes in the height of the upper boundary and in the upper boundary conditions produce small effects in the expected sense, but the cause of the smallness of the response appears to be the high diffusion in the model. In this context notice that

$$\frac{fL}{u\pi} = R_o \approx 0.8$$

where $L \approx 4 \times 10^4$ is the diameter of the eddy, so that advection and rotation operate on comparable time scales, but

$$\frac{\pi K_H}{Lu} \approx 0.4$$

so that diffusion also operates on these time scales and perturbations produced by the hill will be smoothed away. Attempts to reduce the linear diffusion produced unacceptable roughness, but a non-linear diffusion given by

$$\left(\frac{\partial x}{\partial t}\right)_{\text{diffusion}} = K^* \left[\left(\frac{\partial^2 x}{\partial x^2}\right)^3 + \left(\frac{\partial^2 x}{\partial y^2}\right)^3 + \left(\frac{\partial^2 x}{\partial z^2}\right)^3\right]$$

with the value of K^* put equal to 1 (MKS units)
gave the results shown in Fig. 3.3, which are superior to those of Fig. 3.2.

The most interesting aspect of this experiment is the behaviour of the cyclonic eddy formed by the initial movement of air from above the hill to the lee of the hill. It appears that for the present hill's aspect ratio the perturbation velocities produced by the hill

$$\sim \frac{L}{4}\frac{d}{h} f \approx \frac{1}{4} \text{ m sec}^{-1}$$

where d is the height of the hill

are not large enough to trap the cyclone in the vicinity of the hill. For larger hill aspect ratios or larger R_o we would expect the cyclone to rotate round the hill (Huppert & Bryan 1976) and it is intended to discover whether this occurs. It is known that the effects of static stability can affect the magnitude and height variation of the response of a rotating fluid to orography, and this will also be studied.

The second experiment simulated uniform flow with non zero static stability and $f = 0$ past the same isolated hill. The model details are:

grid length = δx = 11 km
horizontal grid of 34 x 36 points
vertical grid of 20 levels whose spacing decreases near the ground
total depth 15.2 km

$f = 0$
$K_H = 0.5 \times 10^4 \text{ m}^2 \text{ sec}^{-1}$ (boundary and interior)
$K_u = 2 \text{ m}^2 \text{ sec}^{-1}$

Again, there are no surface exchanges and the upper and lateral boundary conditions are as described by Tapp and White (1974, 1975) with the modifications mentioned above. There is no high diffusion boundary zone, since the use of such a zone intensified a mild instability at the bounderies. (This instability, which is still evident in the results presented in Fig. 3.4, is suspected to cause some boundary roughness in most integrations of the mesoscale model). The upstream conditions are

$$u = 5 \text{ m sec}^{-1}$$
$$\frac{\partial \theta_1}{\partial z} = 10^{-3} \text{ K m}^{-1} \text{ so } N^2 = \frac{1}{3} \times 10^{-4} \text{ sec}^{-2}$$
$$v = 0$$
$$\dot{\eta} = 0$$

The results at 3 hrs are shown in Fig. 3.4, which shows two vertical cross sections of vertical velocity w (not $\dot{\eta}$) that intersect the hill, one across the flow and one parallel to it. These results seem qualitatively reasonable with the following reservations. The diffusion is again too large, since

$$\frac{\pi K_H}{L u} \approx 0.08$$

In spite of the large diffusion, the rigid lid upper boundary conditions have induced standing waves and this is a problem that must be overcome before any substantial progress can be made since it affects the response to orography in nearly every application of the model. The boundary conditions appear to trap energy or to be unstable at the upstream boundary, which again implies that the present boundary scheme is not adequate. Nevertheless, the slope ($\approx \tan^{-1} 0.071$) of the upstream tilt of the large amplitude stationary response to the hill seems to be close to the theoretical value obtained from linear theory

$$\tan^{-1} \frac{1}{\sqrt{\frac{N^2 L^2}{\pi^2 u^2} - 1}} = \tan^{-1} 0.0685$$

When reasonable solutions are found to the boundary and diffusion problems highlighted by this first experiment, the effect of varying $\frac{NL}{u}$ and $\frac{Nd}{u}$ (d is the height of the hill) will be investigated. The present values were chosen so that the air could pass easily over the hill.

Eventually it is hoped to compare our results with those based on analytical studies of the basic equations eg Scorer (1956). In the meantime, our experiments are providing useful information about general features of the model, eg boundary conditions, as well as testing the ability of the model to respond to orographic features in a qualitatively reasonable way.

4. UK SEA BREEZE FORECAST

The basic version of the mesoscale model, which was originally called the planetary boundary layer model, has been used to "forecast" the development of sea breezes and their associated fronts over the UK on 14 June 1973. Sea breezes were chosen as a test of the model because hydrological effects are not usually important to the formation of sea breeze fronts, and because they are relatively simple and well studied. The date chosen was recommended by Simpson, and is in fact a case that has been studied in detail by Simpson et al (1976). The surface analysis for 00Z, 12Z and 24Z are given in Fig. 4.1.

The initial conditions for the integration of the mesoscale model were obtained by interpolation from a rectangle 10 level model forecast data set for 04Z on 14 June. This relatively coarse resolution (100 km) data was interpolated onto a grid with 61 x 61 points covering England and Wales, a horizontal grid length of 10 km and a total depth of 5 km spanned by 10 irregularly disposed levels. To prevent any sudden shock when the integration started, the field interpolated was the mass field and the hydrostatic relation was assumed.

The Eckman layer equations gave the horizontal winds, and the vertical velocity was given by Richardson's equation, which can be derived by assuming that the time derivative of the hydrostatic relation vanishes. Details of the interpolation and initialisation can be found in Tapp and White (1974).

In order to avoid boundary problems in the initialisation, it is carried out over a larger area than the 61 x 61 pt model area. The boundary values determined during the initialisation are those used throughout the integration. Thus, while the anticyclone in reality moved steadily eastward across the country during the day, the large scale synoptic information supplied to the mesoscale model by the boundary conditions implied a static high pressure cell just to the southwest of the country. The results presented below indicate the importance of correctly varying the boundary conditions, and this will be attempted in the near future.

The formulation of the lateral conditions is not that described in Tapp and White (1974). The method recommended there distinguished between inflow and outflow points and specified the values of all parameters except the pressure at inflow points. When this method was used, the treatment of inflow points proved inappropriate in practice. Because the (initial and constant) boundary value of temperature did not increase through diabatic effects in the same way as the interior values, even over sea points, a vigorous downdraft developed along the eastern part of the northern boundary and the forecast for the whole northeast coast was completely wrong. The present lateral boundary conditions are:

i. the normal velocity is imposed and contstant

ii. the normal derivative of the pressure is calculated from the equation of motion for the normal velocity

iii. for any other field χ, the boundary value $\chi^{(n+1)}$ at time (n+1) is given by

$$\chi_0^{(n+1)} = \chi_0^{(n)} + \chi_2^{(n)} - \chi_2^{(n-1)} \qquad 4.1$$

where $\chi_2^{(n)}$ is the <u>second</u> interior part at time level (n). The choice of the second interior part was necessary for numerical stability at inflow points. Eq 4.1 implies that the long term average of the derivative at the first interior point is constant, since

$$\chi_2^{(n)} - \chi_0^{(n+1)} = \chi_1^{(n-1)} - \chi_0^{(n)} \quad = \text{const}$$

implying

$$\overline{\chi}_2 - \overline{\chi}_0 \quad = \text{const}$$

where the overbar indicates a time average. On shorter time scales, the use

of 4.1 rather than, for example

$$\chi_0^{(n+1)} = \chi_0^{(n)} + \chi_2^{(n+1)} - \chi_2^{(n)}$$

ie $\chi_2^{(n+1)} - \chi_0^{(n+1)}$ = const

implies that waves incident on the boundary from the interior are only partly reflected. Eq 4.1 is also extremely convenient to code.

The upper boundary conditions are those described by Tapp & White (1974).

The principal development of the model needed for this application is a parameterisation of surface exchanges and boundary layer turbulence. This follows the lines suggested in Tapp and White (1974), but since there have been a few modifications the current surface exchanges and boundary layer schemes will be described here.

Surface exchanges of momentum, sensible heat and latent heat, which is required only to complete the surface energy balance, are calculated by bulk transfer formulae

$$\underset{\sim}{\tau} = -\rho C_D |u| \underset{\sim}{u}$$

$$H = -\rho c_p C_H |u| (\theta_1 - \theta_0)$$

$$E = -\rho C_H |u| (q_1 - q_0) \qquad 4.3$$

where $\underset{\sim}{\tau}$ is surface stress

H is sensible heat flux

E is humidity flux

C_D and C_H are bulk transfer coefficients

$\underset{\sim}{u}$ is horizontal velocity at the lowest level

θ_1 is potential temperature at the lowest level

q_1 is humidity at the lowest level (in this case always 10 gm/kg)

θ_0 is surface potential temperature

q_0 is surface humidity

Over the sea, surface temperature is constant and, apart from the calculation of C_D and C_H, 4.3 completes the calculation of the surface fluxes. Over land, the evaporation is limited by the ability of the plants to transpire (Monteith 1974) and surface temperature is determined by the balance of heat flux at the surface. Thus

4.4

$$E = \frac{\varrho (q_{sat}(\theta_0) - q_0)}{r}$$

where r is surface resistance to evapotranspiration.

q_0 can be eliminated from 4.4 and 4.3 to give

$$E = \frac{\varrho C_H |u| (q_{sat}(\theta_0) - q_1)}{1 + r C_H |u|} \qquad 4.5$$

which is the form used in the model. The remaining components of the surface energy balance are:

the heat flux into the ground

$$G = \varrho_s c_s \sqrt{K} \left(h_1 \frac{\partial \theta_0}{\partial t} + h_2 \frac{\partial \theta_s}{\partial t} \right) \qquad 4.6$$

where θ_s is defined by

$$h_2 \frac{\partial \theta_s}{\partial t} = \lambda (\theta_0 - \theta_s)$$

and $\varrho_s c_s \sqrt{K}$ is a constant determined by the nature and condition of the soil and h_1, h_2 and λ are constants chosen so that 4.6 reproduces very closely the behaviour of heat diffusion in an ideal medium. (Eq 4.6 can reasonably be regarded as a two level model for soil heat diffusion, and θ_s as soil temperature)

the solar heating

$$S = 510 \cos(\pi t/12) + 290 \qquad 4.7$$

where t is time measured in hours from midday

thermal heating by the atmosphere

$$B_{\downarrow} = a \sigma \theta_1^4 \quad , \text{ where } a = 0.683 \qquad 4.8$$

(a crude version of the Brunt formula) and the thermal cooling of the surface

$$B_{\uparrow} = \sigma \theta_0^4 \qquad 4.9$$

The surface energy balance equation is

$$B_{\uparrow} + H + LE + G = S + B_{\downarrow} \qquad 4.10$$

where L is latent heat of evaporation

ie

$$\frac{\partial \theta_0}{\partial t} = \frac{[S + B_{\downarrow} - B_{\uparrow} - H - LE]}{\varrho_s c_s \sqrt{K} h_1} - \frac{\lambda}{h_1} (\theta_0 - \theta_s) \qquad 4.11$$

The calculation of the bulk transfer coefficients follows Clarke (1970), so that they are functions of the stability expressed by a bulk Richardson number and a surface roughness length.

The constants that must be specified in order to describe the nature of the surface and use the above equations are a roughness length (z_0) and, over the land only, the surface resistance r and the soil heat capacity parameter $\rho_s c_s \sqrt{K}$. The values used are

$z_0 = 10^{-4}$ m over sea

$z_0 = 10^{-1}$ m over land

$r = 0$ if $E < 0$ (ie dew is forming)

$= 100$ sec m^{-1} during the day

$= 300$ sec m^{-1} during the night

(This is thought to be typical of many trees, but is perhaps a little high for grass)

$$\rho_s c_s \sqrt{K} = 950 \text{ MKS units}$$

(This is thought to be typical of most soils with a reasonable moisture content).

Figure 4.2 shows the variation of the surface heat exchanges through the 24 hours of the model integration at one model point. The sensible heat flux is large but reasonable in view of the clear skies and the time of year. The point that should be emphasized is the importance of the ground heat flux and the fact that no very simple model can be expected to reproduce the timing of the largest ground heat fluxes. The peculiar behaviour of the ground heat flux during the first two hours is due to a poor guess for the initial values for θ_s and should be easy to remove in future experiments.

The parameterisation of boundary layer turbulence in the model has received considerable attention, but not yet a wholly satisfactory solution. Consideration will be given in the near future to the proposals of Busch et al (1976). The use of a high order closure method does not seem appropriate to a model with a 10 km grid length, so the term for boundary layer turbulent diffusion of a general parameter χ are written

$$\left(\frac{\partial \chi}{\partial t}\right)_{\text{turbulent}} = \frac{\partial}{\partial z} K_\chi \frac{\partial}{\partial z} \chi \qquad 4.12$$

which reduces the problem to the specification of K_χ. Close to the surface, K_χ is chosen so that

$$K_\chi \frac{\partial \chi}{\partial z} = \overline{w' \chi'} \qquad 4.13$$

ie the flux of χ is continuous.

Where the surface layer is unstable, it is reasonable to suppose that a well mixed boundary layer with a well defined height and capping inversion will develop, and this situation has been studied by Carson (1973), and Tennekes (1973). It appears that at the top of such a well mixed layer there is a downward flux of heat and that the time development of the well mixed layer is well described if this downward heat flux is related to the upward surface heat flux. In the model context, these ideas are used by

i. diagnosing the highest level within the mixed layer and thus the depth h_x of the well mixed layer

ii. calculating K_θ^x at that level so that a downward heat flux is implied given by

$$K_\theta^x \frac{\partial \theta}{\partial z} = 0.2 H / \rho c_p \qquad 4.14$$

iii. supposing that at the level of the inversion the mixing elements producing the flux of heat are forced from below and mix all other parameters in the same way ie

$$K_\chi^x = K_\theta^x \quad \text{for all } \chi \qquad 4.15$$

Thus, for an unstable surface layer, the depth of layer with large values of K is known and reasonable values for K at the top and bottom of the layer can be calculated.

For stable surface layers there are no such well developed theoretical ideas. Since the initial work with the model used the profile for K suggested by O'Brien (1970), it seems natural to continue with this method in stable conditions. However, in order to ensure that there was no obviously unphysical discontinuity as the surface layer changed between stable and unstable, the ideas described above for the unstable case and the O'Brien profile for the stable case were included in a more general expression. The calculation of K at any height z is given by

$$K = 0.5 \ m^2 \ sec^{-1} \qquad \text{for } z > h'$$

$$K = 0.5 + \left(\frac{h'-z}{h'-h_1}\right)^2 \left(1 + \left(\frac{h'+h_1}{h_1}\right)\left(\frac{z-h_1}{h'-h_1}\right)\right)(K_0 - 0.5) \ m^2 \ sec^{-1} \qquad \text{for } h' > z > h_x$$

$$K = 0.5 + \left(\frac{h'-z}{h'-h_1}\right)^2 \left(1 + \left(\frac{h'+h_1}{h_1}\right)\left(\frac{z-h_1}{h'-h_1}\right)\right)(K_0 - 0.5) + K_x \left(\frac{z-h_1}{h_x-h_1}\right)^2 m^2 sec^{-1} \qquad \text{for } h_x > z > h_1 \qquad 4.16$$

$$K = z/h_1 \ K_0 \ m^2 \ sec^{-1} \qquad \text{for } h_1 > z$$

where

$$h' = h_2 \frac{h^2}{9h_x + 3h_2} + h_x$$

h_1 is the value of z at which Eq.4.13 is imposed

K_0 is the value of K given by Eq.4.13

$h_2 = 25h_1$ ($L = 0.25\ u_*/f$ is the usual notation)

h_x is the depth of the mixed layer as described above

K_x is the value of K given by Eq.4.14

(= 0 for a stable surface layer)

Finally, the diffusion coefficients are enhanced to allow for the effects of shear by adding a small term proportional to the shear.

Figure 4.3 shows the potential temperature profiles given by the model at two grid points close to radiosonde stations. It can be seen that the results are quite good during the day, when the expressions for the diffusion coefficients have some theoretical basis, but less good at nights. A few hodographs have been examined, but their comparison with observations is disappointing, possibly because of the shortcomings of the forecasts as a whole or possibly because of the weak theoretical basis of the above ideas.

The time development of this forecast for 14 June 1973 is shown in Fig. 4.4. The sea breezes form well and move inland in a way typical of these phenomena. Comparison with the results of Simpson et al (1976) and with the operational surface charts indicates that they form about two hours late and remain about two hours behind the actual sea breezes throughout their lifetime. It is possible that this is due to the excessive ground heat flux during the first two hours of the integration. The acceleration of the sea breeze fronts in the evening has also been noted by Simpson et al (1976). The forecast of wind and pressure at 1800 GMT is shown in Fig 4.5.

Fig. 4.6 shows a comparison between the forecast low level winds and the reported winds. The agreement would be outstanding if the forecast winds were all backed through about 20°, and it seems very likely that this disagreement is due to the constant upper and lateral boundary information and the resulting failure to move the anticyclone eastward across the country, or is perhaps due to the difference in height between the model wind (50m) and the observed wind (10m). The lack of progress of the East Anglian sea breeze and the excessive penetrations

of the front originating in the Dee estuary and penetrating the Chessire Gap may also be due to the boundary conditions.

Fig. 4.7 shows a vertical cross section of potential temperature and wind passing N/S just east of Oxford. All the characteristics of sea breeze fronts can be seen, but, because of the resolution of the model, they are often on the wrong scale. This cross section shows the upstream tilt of the gravity waves set up by the front, which is possible in spite of the rigid upper lid because of high diffusion in the model.

Fig. 4.8 shows the effect of including orography in the model. When comparing these two integrations three factors should be noted:

i. the model is only 4 km deep so many effects due to orography could be exaggerated.

ii. the sensible heat flux is increased by raising the height of the surface, so the sea breeze effects should be stronger in the presence of orography.

iii. the upper boundary conditions hold horizontal winds constant at inflow points so that, at that level for inflow points, the air is forced to pass over rather than round hills.

Nevertheless, the cyclonic eddy in the northeast is a reasonable effect of orography, although probably forecast at the wrong time and with the wrong magnitude. The orography itself is shown in Fig. 4.9.

This simulation of real conditions by the mesoscale model is very encouraging, but it must be stressed that the situation is particularly simple. The most notable fact is that a detailed forecast was produced from very smooth initial data that disregarded the large amount of information which is routinely available. For this situation, the weather is determined by the large scale synoptic situation and the boundary layer forcing rather than local past events, ie, in model terms, the boundary conditions are more important than the initial conditions. Since the upper and lateral boundary conditions can be supplied by larger scale models, but initial conditions might require the complicated analysis of conventional and unconventional observations this is encouraging.

5. THE CUMULUS MODEL

A full description of this development of the mesoscale model has been given by Tapp (1977). The bulk of this section shows how the basic equations are extended to include the extra fields and processes involved in convection. The last part describes an attempt to verify the model by repeating a study already carried out by Bennetts (1977).

The original equations for dry air have been extended to include water vapour, cloud water and rain water. Three extra continuity equations express the conservation of these three parameters, with source and sink term that model microphysical terms, which are believed to be important in cumulus and cumulonimbus. In order to render this four component system tractable, the velocities of air, water vapour and cloud water are assumed identical ($= \underset{\sim}{u}$), and rain water is assumed to have a fall velocity ($= \underset{\sim}{u}_T$) (positive downward) relative to the other components. $\underset{\sim}{u}_T$ is assumed to be a function of the rain water mixing ratio only

$$u_T = 21.18\, r^{.2} \text{ m sec}^{-1} \qquad 5.1$$

where r is mass of rain water per unit mass of dry air.

The continuity equations for vapour (x), cloud water (c) and rain water (r) are:

$$\frac{Dx}{Dt} = S_x$$

$$\frac{Dc}{Dt} = S_c$$

$$\frac{Dr}{Dt} - u_T \frac{\partial r}{\partial t} - \frac{r}{\rho} \cdot \frac{\partial}{\partial z} \rho u_T = S_r \qquad 5.2$$

where x, c and r are mixing ratios per unit mass of dry air and S_x, S_c and S_r are source and sink terms that will be discussed below.

The momentum equations are derived in the usual way

$$(1+x+c+r)\frac{D\underset{\sim}{u}}{Dt} + r\left(\frac{D\underset{\sim}{u}_T}{Dt} - u_T \frac{\partial}{\partial z}(\underset{\sim}{u} + \underset{\sim}{u}_t)\right)$$

$$+ \underset{\sim}{u}_T S_r = -(1+x+c+r)g - \frac{1}{\rho}\nabla p \qquad 5.3$$

where ρ is the density of dry air. If the Exner function is defined as for the equations for dry air

$$\Pi = (p/p_r)^K = \left(\frac{p_d + e}{p_r}\right)^K \qquad 5.4$$

where p_d is the pressure of dry air and.
e is the pressure of water vapour

then

$$\frac{1}{\rho}\nabla p = \left(1 + \frac{e}{p_d}\right) c_p \theta \nabla \Pi = (1 + 1.61x) c_p \theta \nabla \Pi \qquad 5.5$$

Equation 5.3 is now simplified by noting

$$x, c, r << 1$$

and

$$c_p \theta \nabla P \approx -g$$

so that

$$\frac{1+1.61x}{1+x+c+r} c_p \theta \nabla P \approx c_p \theta \nabla P + (.61x - c - r) c_p \theta \nabla P$$

$$\approx c_p \theta \nabla P - (.61x - c - r)\, g \qquad 5.6$$

and only the lowest order approximations to the term involving u_T need be retained. Then 5.3 becomes

$$\frac{Du}{Dt} - r u_T \frac{\partial u}{\partial z} = - c_p \theta \frac{\partial P}{\partial x}$$

$$\frac{Dv}{Dt} - r u_T \frac{\partial v}{\partial z} = - c_p \theta \frac{\partial P}{\partial y}$$

$$\frac{Dw}{Dt} - r u_T \frac{\partial v}{\partial z} + r \left(v_T \frac{\partial u_T}{\partial z} - \frac{D u_T}{Dt} - \frac{u_T S_r}{r} \right)$$

$$= - g (1 - .61x + c + r) - c_p \theta \frac{\partial P}{\partial z} \qquad 5.7$$

In equations 5.7 the effect of the water variables on the buoyancy of the mixture is transparent.

The thermodynamic equation is obtained by approximating the enthalpy per unit mass of dry air

$$H = c_p T + L x \qquad 5.8$$

and noting that

$$\frac{DH}{Dt} = Q + \frac{1}{\rho} \frac{Dp}{Dt} = Q + c_p \theta \frac{DP}{Dt} \qquad 5.9$$

(to the same level of approximation as 5.8) where Q is the diabatic heating. Simple algebra gives

$$\frac{D\theta}{Dt} = \frac{1}{c_p P} \left(Q - L \frac{Dx}{Dt} \right) \qquad 5.10$$

Finally, the continuity equations for dry air give the prognostic equations for P

$$\frac{DP}{Dt} + (\gamma - 1) P \nabla \cdot \underset{\sim}{u} = \frac{(\gamma - 1) P}{\theta} \left(\frac{D\theta}{Dt} + 1.61 \theta \frac{Dx}{Dt} \right) \qquad 5.11$$

where terms of order x^2 have been neglected.

The cloud physics terms S_x, S_c and S_r are parameterised in a similar way to that of Liu and Orville (1969) and Miller and Pearce (1974).

$$S_x = -P_1 + P_2 + P_3 \qquad 5.12$$

where

$$P_1 = -\beta (x - x_{sat})$$

$$\text{or } 0 \quad \text{for } x > x_{sat} \qquad 5.13$$

is the evaporation of raindrops.

$$P_2 = \gamma c r^{.95} \qquad 5.14$$

is the conversion of cloud to rain by accretion and

$$P_3 = \alpha (c - c_{crit})$$

$$\text{or } 0 \quad \text{for } c < c_{crit} \qquad 5.15$$

is the autoconversion of cloud to rain. Note that P_1, P_2 and P_3 are all positive or zero.

$$S_c = -P_2 - P_3 + S_{c/e}$$

$$S_x = P_1 - S_{c/e} \qquad 5.16$$

where $S_{c/e}$ is the evaporation or condensation of cloud and is calculated by assuming that the air never becomes supersaturated and that cloud is instantly evaporated in an unsaturated environment.

The present values of the constants are

$$\alpha = 10^{-3} \text{ sec}^{-1}$$
$$\beta = 10^{-3} \text{ sec}^{-1}$$
$$\gamma = 707.95 \times 10^{-3} \text{ sec}^{-1}$$
$$c_{crit} = 5 \times 10^{-4} \text{ gm/kg}$$

Figure 5.1 illustrates the microphysical processes.

The finite differences approximations to these equations is the same as that for the basic dry model except in respect of the advection of cloud and rain. When the usual second order accurate centred calculations were used for these very localized fields, large negative values quickly accumulated and so a first order accurate quasi-Lagrangian advection scheme is used for these parameters only. The form of diffusion used to control grid scale roughnesses in this version of the model is calculated as

$$K_H |\nabla_H^2 \chi| \nabla_H^2 \chi + K_v \left|\frac{\partial^2 \chi}{\partial z^2}\right| \frac{\partial^2 \chi}{\partial z^2}$$

where χ is any of the fields u, θ and x and ∇_H^2 is the two dimensional horizontal Laplacian. The remaining fields P, c and r are not smoothed.

The original formulation for the upper and lateral boundary conditions was that reported by Tapp and White (1974). Since all the velocities vanished on the boundaries, they were treated as inflow points and the values of tangential velocity, θ, c and r were held constant. This formulation proved unstable, and so all the boundary points were treated as outflow but otherwise as in Tapp and White (1974). Thus the boundary value of potential temperature is determined by upstream advection, the normal derivative of pressure is determined the momentum equations, the normal velocity vanishes and all other boundary values are put equal to the first interior value at the previous time step. There have been no further computational problems due to these boundary conditions, but the only guarantee that wave energy is propagated out of the integration region is a high diffusion zone.

The model that has been described above is being used to study the convection that occurs in the environment illustrated in Fig. 5.2. In order to initiate the ascent of surface air, heat and moisture are injected into the bottom two levels. This is maintained for 45 mins and is such as to produce a warming of $2^{\circ}C$ over the central four points and 1° elsewhere and a moistening of 1 gm/kg over the central four points.

The resulting convection is illustrated in Fig. 5.3 to Fig. 5.6. According to Bennetts (private communication), the striking feature of these results is their similarity with those obtained using the Miller and Pearce (1974) model, which are described by Bennetts (1977). In particular, the formation of a cold descending cell beneath the first bubble is a very familiar problem and is probably explained by the entrainment of relatively cold environment air as the first bubble rises. This could possibly be avoided by initiating the ascent in a more realistic way. The cold downdraft suppresses the development of a second ascending bubble, which, in the results of Bennetts (1977), plays a

crucial role in the development and increased lifetime of the cumulus cloud. Insofar as a second bubble does show in the present results, its vertical and horizontal scales appear to be mutually related and related to those of the first bubble, as occurs in the results of Bennetts (1977). The rain in the present results develops rather early, but this is probably not the cause of the cold downdraft, and can be explained by the low value of C_{crit} (the value of C at which autoconversion to rain begins).

It is planned to change the method of initiation by imposing a low level convergence and applying no preferential heating at the centre of the grid. In this way it is hoped that the initial bubble will form on some internally determined scale and that the problem caused by the entrainment of cold air will be avoided by slowing down the initial release of the bubble or by ensuring that the entrained environment air is relatively warm.

The similarity between the behaviour of the present model and that of Miller and Pearce (1976) must be encouraging for both models. The formulation of the dynamics of the models are almost as different as possible, so it is unlikely that the common results are due to some common peculiarity rather than a common simulation of reality. However, it must be pointed out that quite marked changes can be produced in the present model (and probably in the Miller and Pearce model) by apparently trivial changes in a few finite difference approximations. Thus the similarity could be made even more marked or possibly be persuaded to disappear by judicious "tuning" of the details of either model.

The future use of this cumulus model will probably be to study the interactions between the boundary layer and clouds, in particular the role of a well developed boundary layer in supercell storm or the development of moderate cumulus and stratocumulus beneath a well defined inversion. It could also be used in several ways to provide valuable guidance covering the parameterisation of convection in larger scale models.

APPENDIX 1

Tapp and White have already discussed the use of an implicit time stepping scheme for the sound waves in the mesoscale model. This method leads to a Helmholtz equation for a form of the pressure field that was originally solved by Alternating Direction Implicit (ADI) iterative techniques. In this Appendix the direct method of solutions recently developed by Tapp (1976) is briefly described. For completeness, the earlier work leading to the Helmholtz equations is repeated here.

The basic model equations 2.1 can be written in a form that emphasises the existence of sound waves as solutions.

$$\frac{\partial u}{\partial t} = -c_p(\theta_0+\theta_1)\frac{\partial P_1}{\partial x} + X$$

$$\frac{\partial w}{\partial t} = -c_p(\theta_0+\theta_1)\frac{\partial P_1}{\partial z} + Z$$

$$\frac{\partial P_1}{\partial t} = \frac{g w}{c_p \theta_0} - (\gamma-1)(P_0+P_1)\left(\frac{\partial u}{\partial x}+\frac{\partial w}{\partial z}\right) + R \qquad \text{A.1}$$

where X, Z and R contain the remaining terms, which are all calculated by an explicit time stepping scheme. The finite difference approximation in time to A.1 is

$$u^{(n+1)} - u^{(n-1)} = -2\delta t\left\{c_p\theta_0 \tfrac{1}{2}\left(\frac{\partial P_1^{(n+1)}}{\partial x}+\frac{\partial P_1^{(n-1)}}{\partial x}\right) + c_p\theta_1\frac{\partial P_1^{(n)}}{\partial x} - X\right\}$$

$$w^{(n+1)} - w^{(n-1)} = -2\delta t\left\{c_p\theta_0 \tfrac{1}{2}\left(\frac{\partial P_1^{(n+1)}}{\partial z}+\frac{\partial P_1^{(n-1)}}{\partial z}\right) + c_p\theta_1\frac{\partial P_1^{(n)}}{\partial z} - Z\right\}$$

$$P_1^{(n+1)} - P_1^{(n-1)} = -2\delta t\left\{-\frac{g}{c_p\theta_0}\frac{w^{(n+1)}+w^{(n-1)}}{2} + (\gamma-1)P_0\tfrac{1}{2}\left[\left(\frac{\partial u}{\partial x}+\frac{\partial w}{\partial z}\right)^{(n+1)} + \left(\frac{\partial u}{\partial x}+\frac{\partial w}{\partial z}\right)^{(n-1)}\right] + (\gamma-1)P_1\left(\frac{\partial u}{\partial x}+\frac{\partial w}{\partial z}\right)^{(n)} - R\right\} \qquad \text{A.2}$$

Note the separation of the pressure gradient and divergence terms into those parts that are present in the basic atmosphere, which are treated implicitly, and those parts that depend on the perturbations θ_1 and P_1, which are treated explicitly. The manipulation of these equations is simplified by introducing a second order correction (in time) field Π

$$\pi(t) = c_p \theta_0 \left(P_1(t+\delta t) - 2P_1(t) + P_1(t-\delta t) \right)$$

$$= c_p \theta_0 \left(P_1^{(n+1)} - 2P_1^{(n)} + P_1^{(n-1)} \right)$$

A.3

Substituting A.3 in A.2

$$u^{(n+1)} - u^{(n-1)} = -2\delta t \frac{\partial \pi}{\partial x} - 2\delta t \left\{ c_p (\theta_0 + \theta_1) \frac{\partial P_1^{(n)}}{\partial x} - X \right\}$$

$$w^{(n+1)} - w^{(n-1)} = -2\delta t \frac{\partial \pi}{\partial z} - 2\delta t \left\{ c_p (\theta_0 + \theta_1) \frac{\partial P_1^{(n)}}{\partial z} - Z \right\}$$

$$\frac{\pi}{c_p \theta_0} + 2\left(P_1^{(n)} - P_1^{(n-1)} \right) = \text{r.h.s. as in A.2} \qquad \text{A.4}$$

Now the unknown fields $u^{(n+1)}$, $w^{(n+1)}$ can be eliminated to obtain

$$\nabla_H^2 \pi + \left\{ \frac{\partial^2}{\partial z^2} - \frac{g}{c_0^2} \frac{\partial}{\partial z} - \frac{1}{c_0^2 \delta t^2} \right\} \pi = G \qquad \text{A.5}$$

where

$$c_0^2 = (\gamma - 1) c_p \theta_0 P_0$$

and G can be evaluated using the field values at the current and previous time step. If A.5 is solved, the future values of u, v and w are given by A.4 and the future value of P_1 is given by A.3.

When the $\partial/\partial z$ terms are approximated by finite differences, A.5 can be written

$$\nabla_H^2 \underset{\sim}{\pi} - \underset{\approx}{A}\, \underset{\sim}{\pi} = \underset{\sim}{G} \qquad \text{A.6}$$

where $\underset{\sim}{\pi}$ is a column vector of values at the model levels and

$\underset{\approx}{A}$ is the matrix representation of the operator

$$- \left\{ \frac{\partial^2}{\partial z^2} - \frac{g}{c_0^2} \frac{\partial}{\partial z} - \frac{1}{c_0^2 \delta t^2} \right\}$$

Tapp and White (1974, 1975) described how A.6 can be reduced to a set of independent two dimensional Helmholtz equations

$$\nabla_H^2 \rho_i - \lambda_i \rho_i = \beta_i \qquad \text{A.7}$$

by introducing a matrix $\underset{\approx}{H}$ such that

where $$\underset{\approx}{H}\ \underset{\approx}{A}\ \underset{\approx}{H}^{-1} = \text{diag}\,(\lambda)$$

and $$\underset{\sim}{\eta}^{(i)}\ \underset{\approx}{A} = \lambda_i\ \underset{\sim}{\eta}^{i}$$

$$\underset{\sim}{\rho} = \underset{\approx}{H}\ \underset{\sim}{\Pi}$$

The original ADI solution of A.7 had two disadvantages that were mentioned in the text. The reason for the second disadvantage, ie the failure of the iterative procedure to converge when the aspect ratio of the grid was varied, can be explained using A.7. The ADI method requires a "first guess" solution and the simple choice is

$$\rho_i = -\beta_i / \lambda_i \qquad \text{A.8}$$

For a horizontal grid length of 10 km and a total model depth of 4 km

$$\nabla_H^2 / \lambda_i < \text{or} \approx \tfrac{1}{2}$$

and A.8 gives a good first guess solution for A.7. However, when the horizontal grid length is decreased to 1 km and the total model depth is increased to 15 km

$$\nabla_H^2 / \lambda_i < \text{or} \approx 400$$

and it is no longer easy to find an approximation to ρ_i. A.8 can be written

$$\underset{\approx}{Y}\ \underset{\approx}{\rho} + \underset{\approx}{\rho}\ \underset{\approx}{X} - \lambda\ \underset{\approx}{\rho} = \underset{\approx}{\beta} \qquad \text{A.9}$$

where the matrix notations now refer to horizontal arrays, so that

$$\left(\underset{\approx}{\rho}\right)_{m,n} = \rho_{m\,n}$$

where ρ_{mn} is the value of ρ at grid point m in the y directions and n in the x direction. The simplicity of the direct method of solving A.9 is due to two facts:

i. λ is independent of x, y.

ii. $\underset{\approx}{X}$ and $\underset{\approx}{Y}$ which respresent $\frac{\partial^2}{\partial x^2}$ and $\frac{\partial^2}{\partial y^2}$ are tri-diagonal matrices

A matrix $\underset{\approx}{E}$ is sought such that

$$\underset{\approx}{E}^{-1}\ \underset{\approx}{X}\ \underset{\approx}{E} = \mathrm{diag}(\mu) \qquad \text{A.10}$$

where μ are the eigenvalues of $\underset{\approx}{X}$, and A.9 is manipulated

or if $$\underset{\approx}{Y}\ \underset{\approx}{\rho}\ \underset{\approx}{E} + \underset{\approx}{\rho}\ \underset{\approx}{E}\ \underset{\approx}{E}^{-1}\ \underset{\approx}{X}\ \underset{\approx}{E} - \lambda\ \underset{\approx}{\rho}\ \underset{\approx}{E} = \underset{\approx}{\beta}\ \underset{\approx}{E}$$

$$\underset{\approx}{\phi} = \underset{\approx}{\rho}\ \underset{\approx}{E}$$

and $$\left(\underset{\approx}{\phi}\right)_{mn} = \left(\underset{\sim}{\phi}^{(n)}\right)_m$$

$$\underset{\approx}{Y}\ \underset{\sim}{\phi}^{(n)} - \mu_n \underset{\sim}{\phi}^{(n)} - \lambda\ \underset{\sim}{\phi}^{(n)} = \underset{\sim}{\gamma}^{(n)} \qquad \text{A.11}$$

where $\gamma^{(n)}$ is defined by

$$\left(\underset{\sim}{\gamma}^{(n)}\right)_m = \left(\underset{\approx}{\beta}\ \underset{\approx}{E}\right)_{mn} \qquad \text{A.12}$$

For any row m of data the values of $\left(\underset{\sim}{\gamma}^{(n)}\right)_m$ can be calculated at the same time as the explicit parts of the time stepping increments. This simplifies the computer coding of the model because the program is written so that only a limited number of whole rows of data are in main storage simultaneously.

The derivation of A.11 and A.12 has been expressed in general matrix terms, as was the decoupling of the vertical operator $\underset{\approx}{A}$ in equation A.6. However, A.12 can be expressed as a Fourier transform in the x direction and equation A.11 is merely the Fourier transform of equation A.9. The potential efficiency of the direct method is realised by using Fast Fourier Transform techniques to transform the r.h.s. of equation A.11 and to reconstitute the solution to A.11.

Equation A.11 is solved by noting that $\underline{\underline{Y}}$ is tridiagonal. If

$$\underline{\underline{Y}} = \begin{pmatrix} \ddots & & & & \\ & Y_0 & Y_+ & 0 & 0 \\ & Y_- & Y_0 & Y_+ & 0 \\ & 0 & Y_- & Y_0 & Y_+ \\ & 0 & 0 & Y_- & Y_0 \ddots \end{pmatrix}$$

A.11 can be written

$$Y_+ \phi^{(n)}_{m+1} + Y_0 \phi^{(n)}_m + Y_- \phi^{(n)}_{m-1} - (\mu_n + \lambda)\phi^{(n)}_m = \gamma^{(n)}_m$$

which gives

$$\phi^{(n)}_m = a^{(n)}_m \phi^{(n)}_{m+1} + b^{(n)}_m \qquad \text{A.14}$$

where

$$a^{(n)}_m = - \frac{Y_+}{Y_0 + a^{(n)}_{m-1} Y_- - \mu_n - \lambda}$$

and

$$b^{(n)}_m = \frac{Y_- b^{(n)}_{m-1} - \gamma^{(n)}_m}{Y_+} a^{(n)}_m$$

The sequences $\{a\}, \{b\}$ can be calculated inductively, and then the solution $\{\phi\}$ can also be calculated inductively. The boundary conditions determine the initial values for these series. This method, which is a special adaption of Gaussian elimination, is often referred to as the "double sweep method".

References

Bennetts, D. A. (1977)

"A numerical study of the initiation and early development of convection in temperate latitudes" to appear in Q.J. Roy. Met. Soc.

Busch, N. E., Chang, S.W. and Anthes R. A. (1976)

"A multilevel model of the planetary boundary layer suitable for use with mesoscale dynamic models"

Journ. App. Met., 15

Carson, D. J. (1973)

"The development of a dry inversion capped convectively unstable boundary layer"

Q. J. Roy. Met. Soc. 99

Clarke, R. H. (1970)

"Recommended methods for the treatment of the boundary layer in numerical models".

Aust. Met. Mag 18

Huppert, H. E. and Bryan, K. (1976)

"Topographically generated eddies"

Deep Sea Res. 23

Liu, J. Y. and Orville, H. D. (1969)

"Numerical modelling of precipitation and cloud shadow effects on mountain - induced cumuli"

Journ. Atmos. Sci., 26

Miller, M. J. and Pearce, R. P. (1974)

"A three dimensional primitive equation model of cumulonimbus convection"

Q. J. Roy. Met. Soc., 100

Monteith, J. L. (1964)

"Evaporation and environment"

Symp. Soc. Exp. Bio 19

O'Brien, J. J. (1970)

"A note on the vertical structure of the eddy exchange coefficient"

Jour. Atmos. Sci 27

Scorer, R. S. (1956)

"Airflow over an isolated hill"

Q. J. Roy. Met. Soc., 82

Simpson, J. E., Mansfield, D. A. and Milford, J. R. (1977)

"Inland penetration of sea breeze fronts"

Q. J. Roy. Met. Soc. 103

Tapp, M.C. and White, P. W. (1974)

"The planetary boundary layer model" - Basic formulation

Met.O.11 Technical Note No.46

Tapp, M. C. and White, P. W. (1976)

"A non hydrostatic mesoscale model"

Q J Roy. Met. Soc. 102

Tapp, M. C. (1976)

"A direct method for the solution of Helmholtz-type equations"

Met O 11 Tech. Note No. 71

Tapp, M. C. (1977)

"Cumulus modelling using the mesoscale model"

Met O 11 Tech. Note No. 79

Tennekes, H (1973)

"A model of the dynamics of the inversion above a convective boundary layer"

Journ. Atmos. Sci. 30

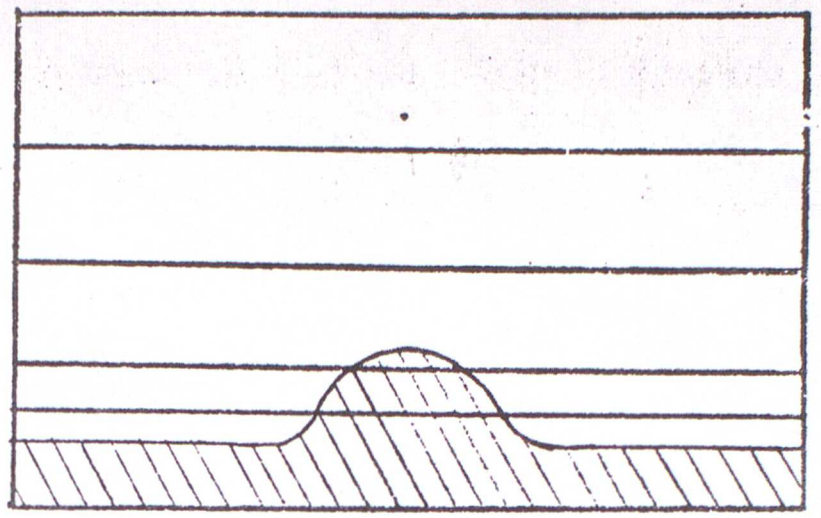

A

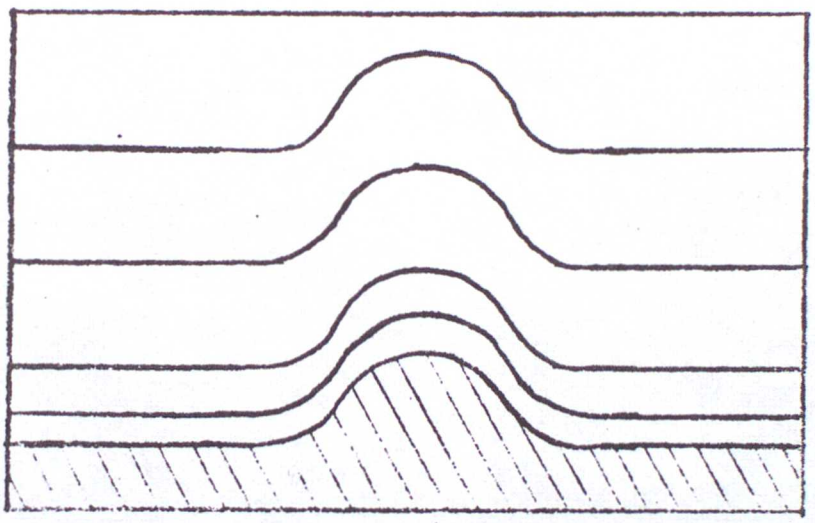

B

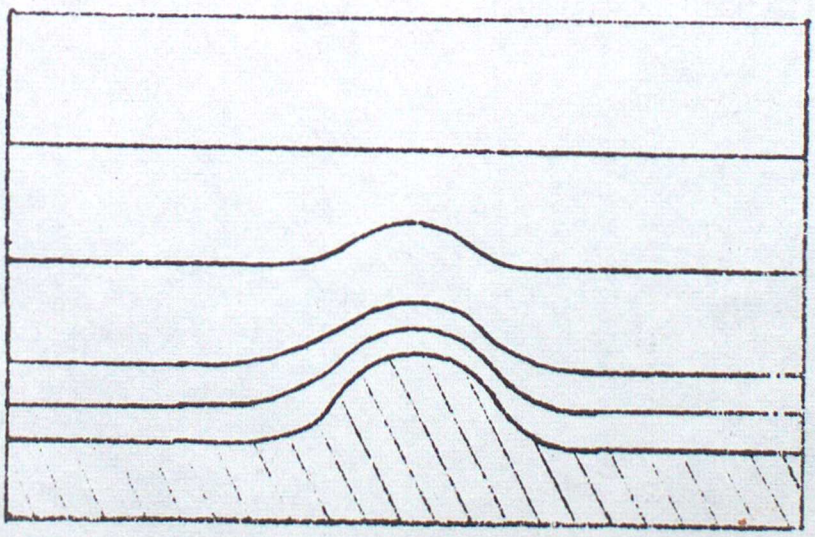

C

Fig. 3.1

Three possibilities for the disposition of model levels in the presence of orography.

Fig. 3.2

The perturbation of uniform isotropic flow past an isolated hill after 3 hrs and 6 hrs. Roughness was controlled by linear diffusion with a Reynolds number near unity.

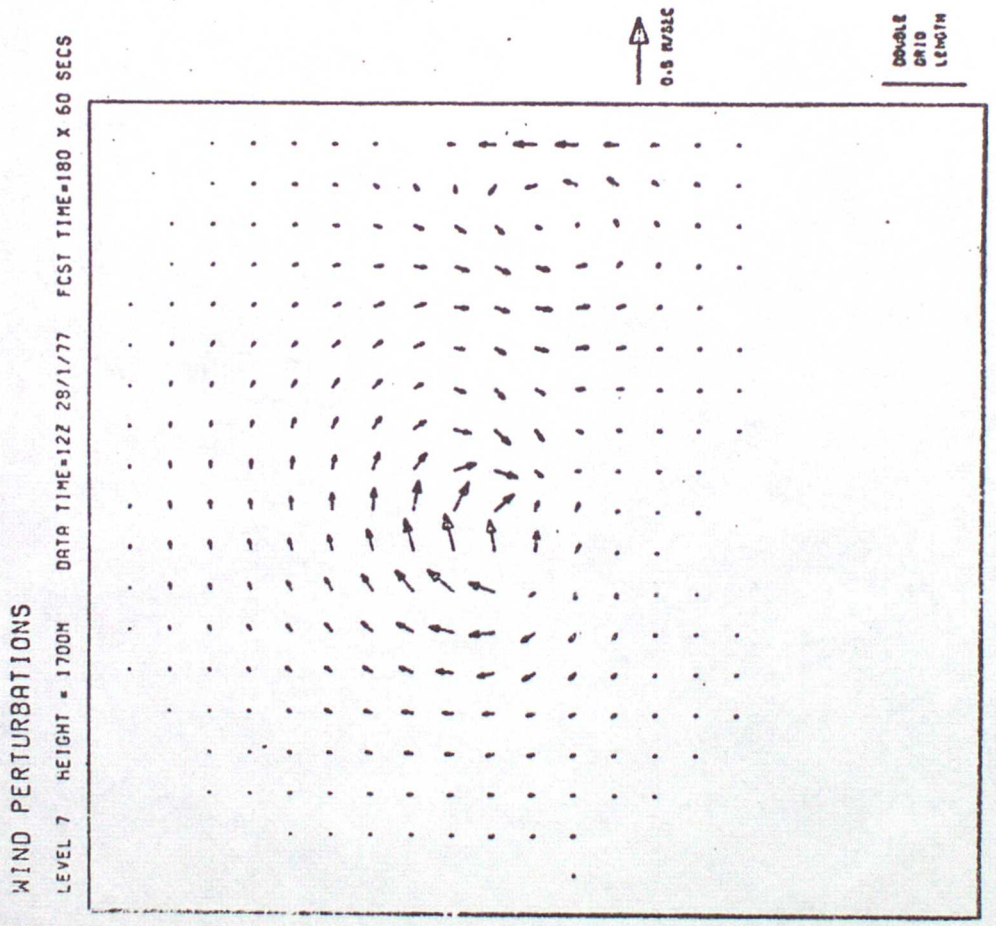

Fig. 3.3

The perturbation of uniform isotropic flow past an isolated hill after 3 hrs. Roughness was controlled by a non linear, non isotropic diffusion that selectively damped short wave length features.

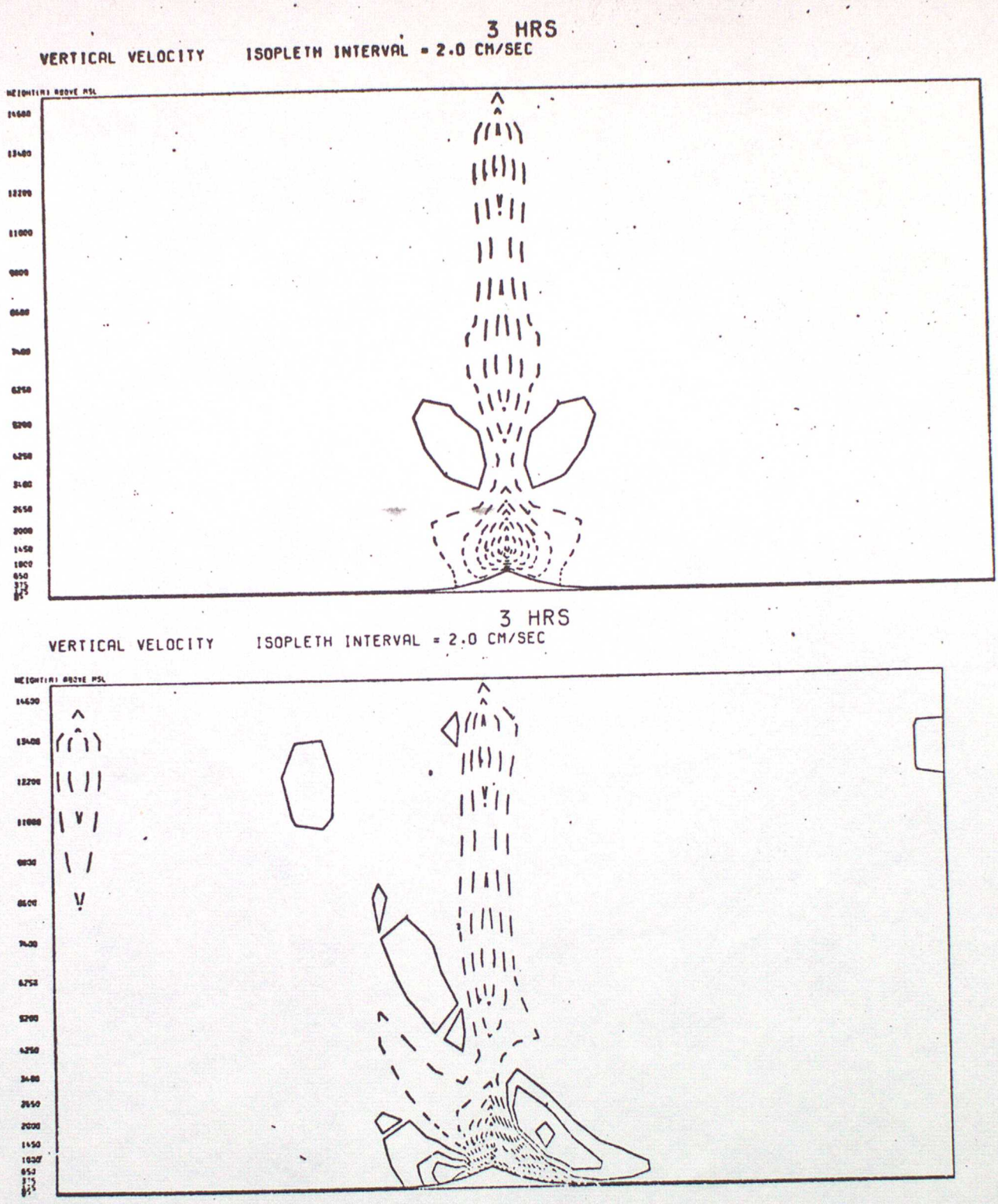

Fig. 3.4

Cross sections showing vertical velocity induced by statically stable uniform flow over an isolated hill. The top section is across the flow and the bottom section is parallel to the flow.

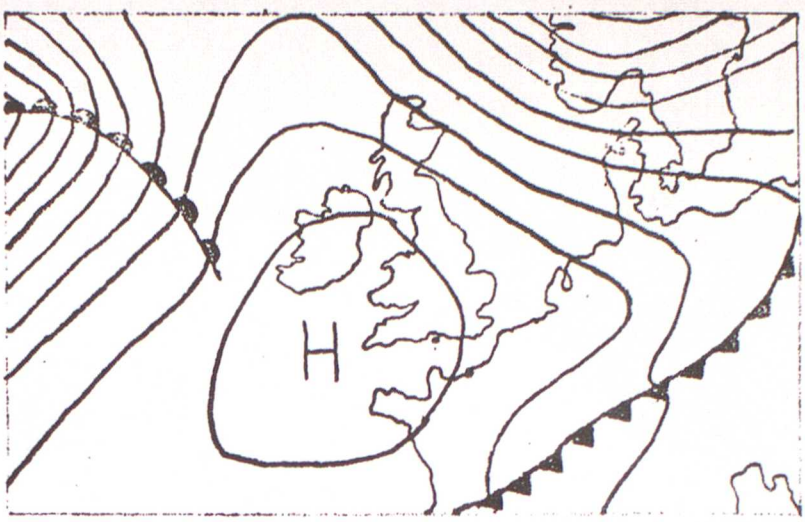

0000 G.M.T.

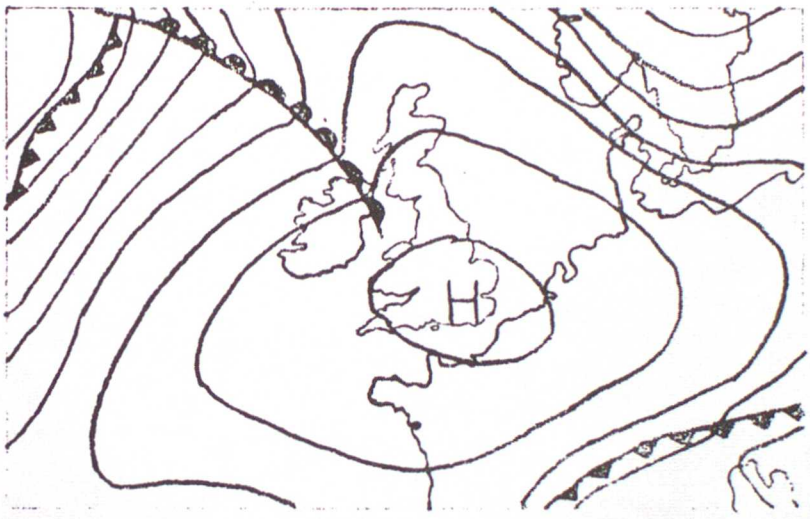

1200 G.M.T.

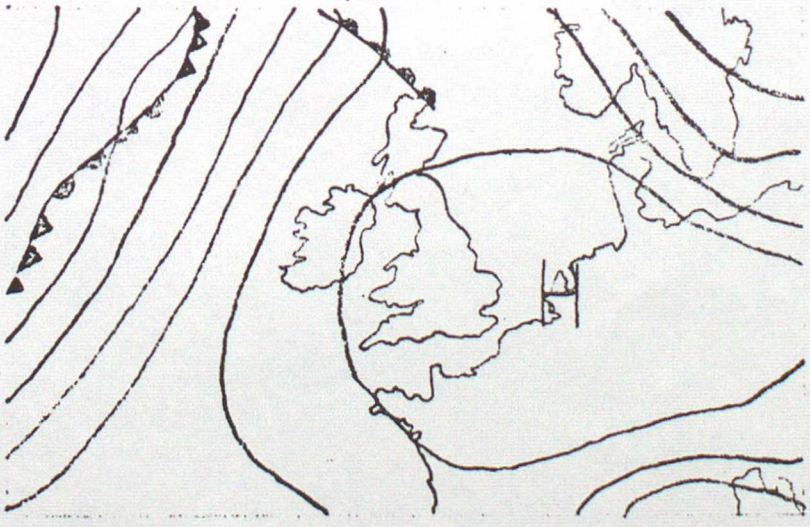

2400 G.M.T.

Fig. 4.1

The synoptic situation over the UK on 14 June 1973

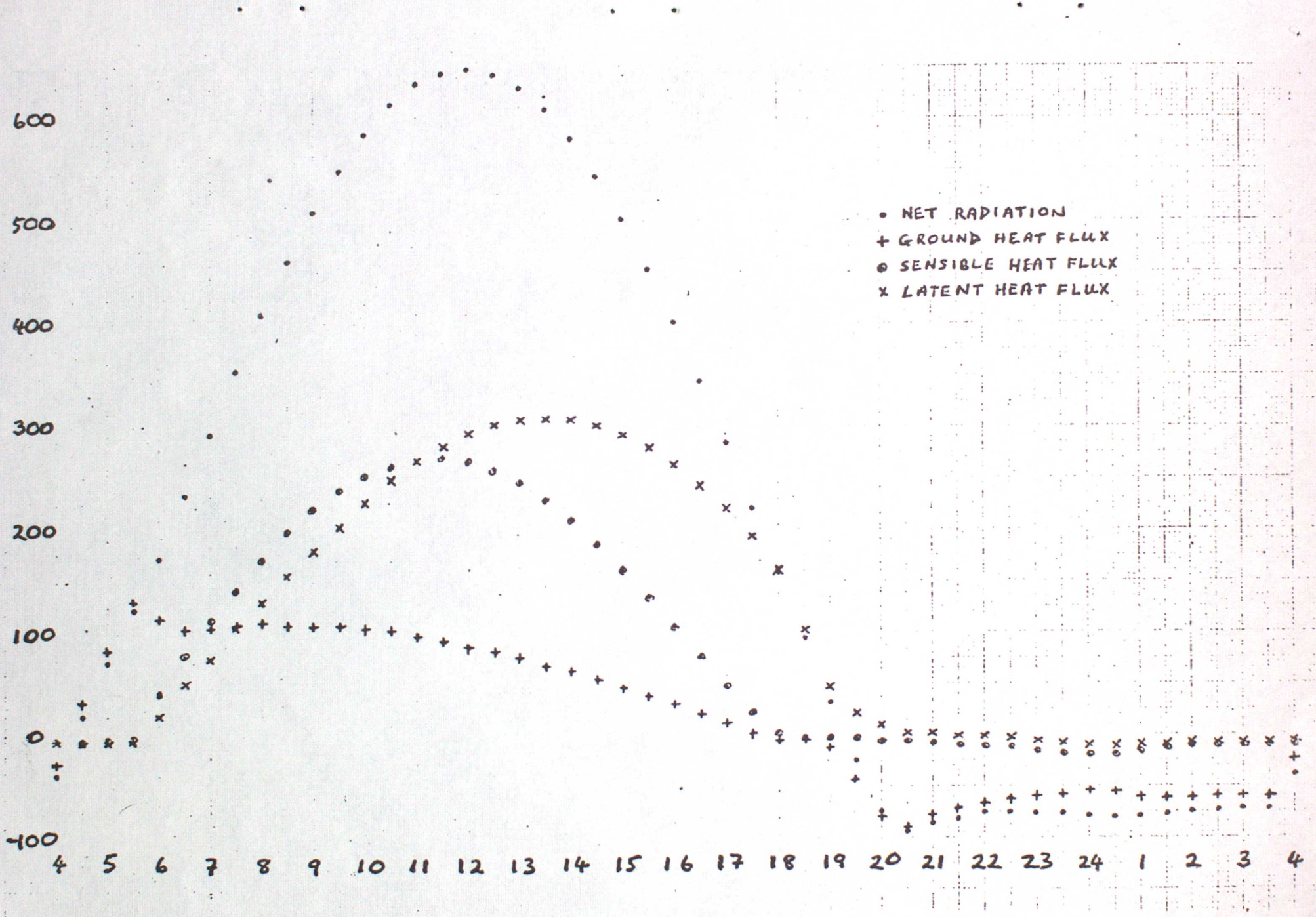

Fig. 4.2

The surface heat budget given by the model for a point in the Midlands.

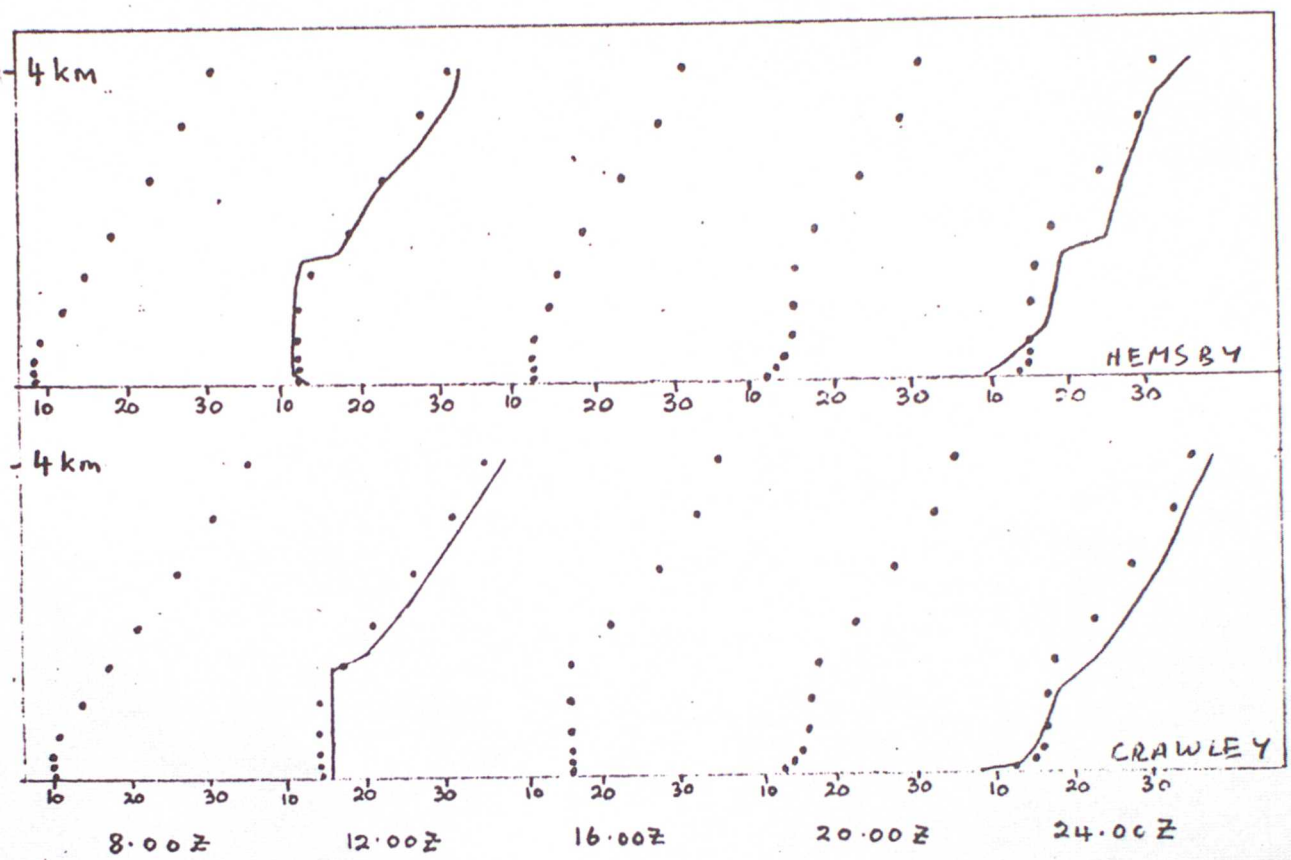

Fig. 4.3

Potential temperature at each of 10 model levels at 4 hour intervals for Hemsby and Crawley. The solid lines at 12Z and 24Z are the routine radiosonde observations

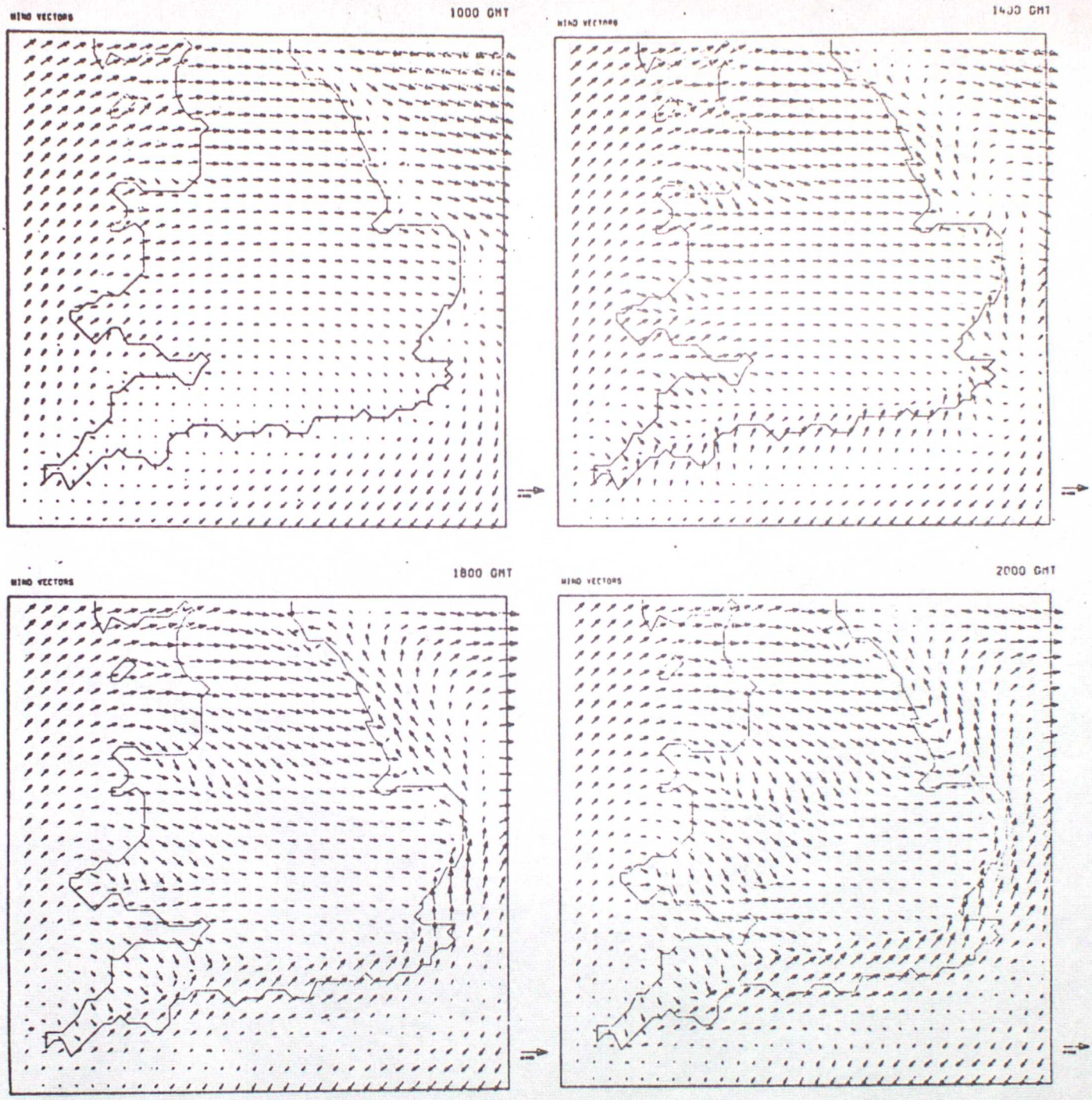

Fig. 4.4

Forecast winds at 50 m for 1000, 1400, 1800 and 2000 GMT 14 June 1973 for the model without orography. Note the reduced interval between the last two times.

1800 GMT

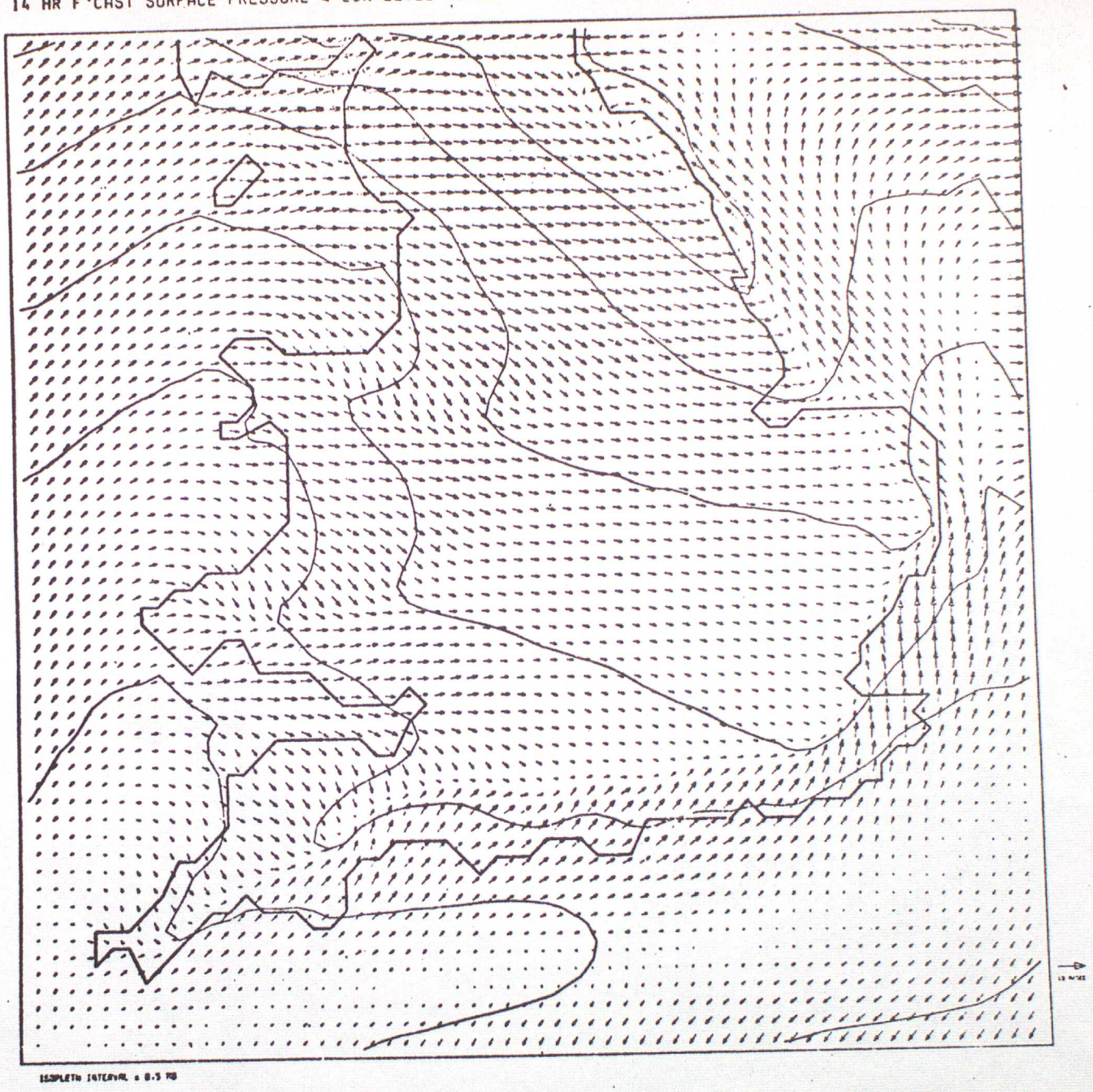

Fig. 4.5

Winds and pressure forecast for 1800 GMT if orography is not included in the model.

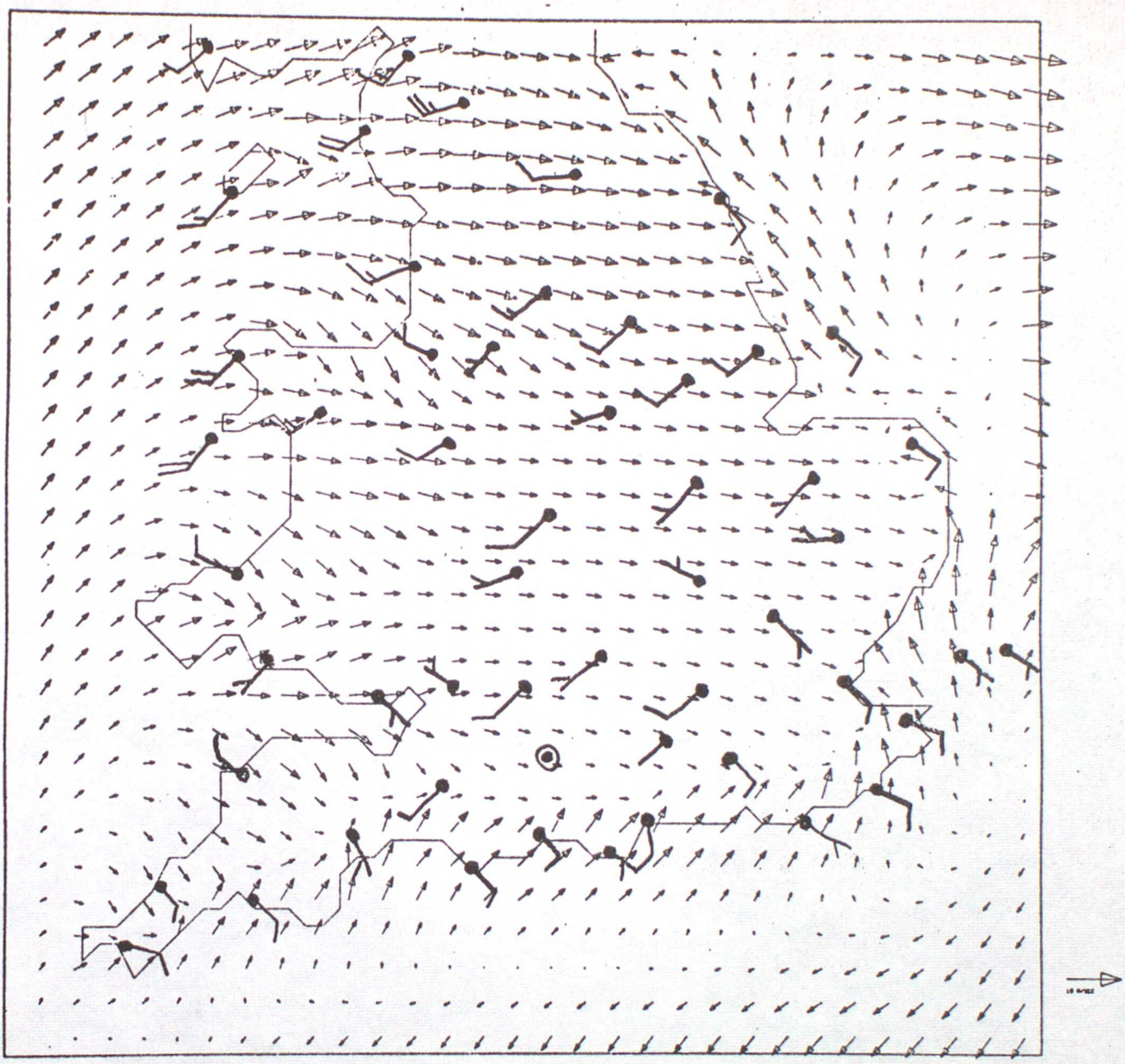

Fig. 4.6

Forecasts of wind (by the model without orography) at 50 m (the lowest model level) for 1600 GMT on 14 June 1973 are shown by arrows. The arrow in the key shows 10m sec^{-1}. The routine surface wind observations are shown in the usual way.

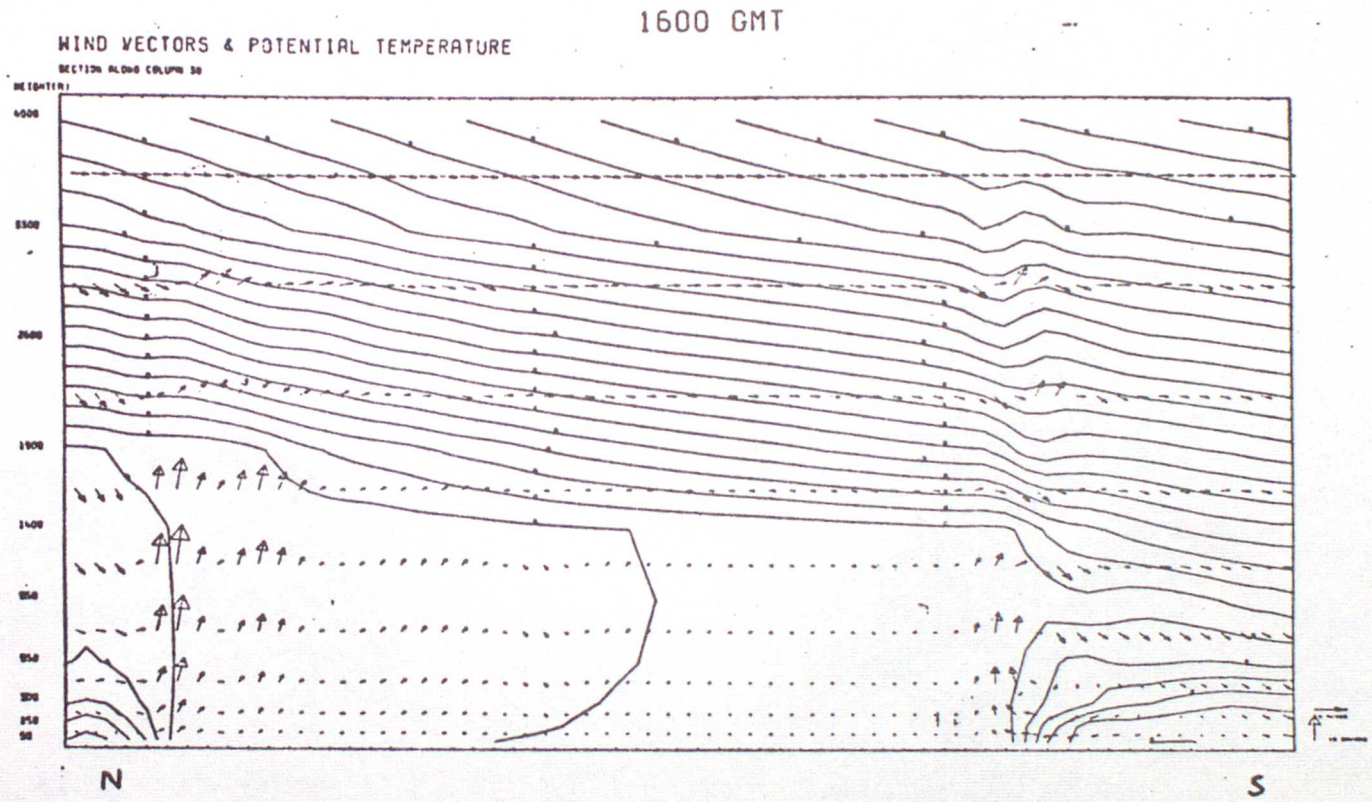

Fig. 4.7

Vertical cross section showing forecast wind and potential temperature along a line passing N/S just east of Oxford and the Isle of Wight.

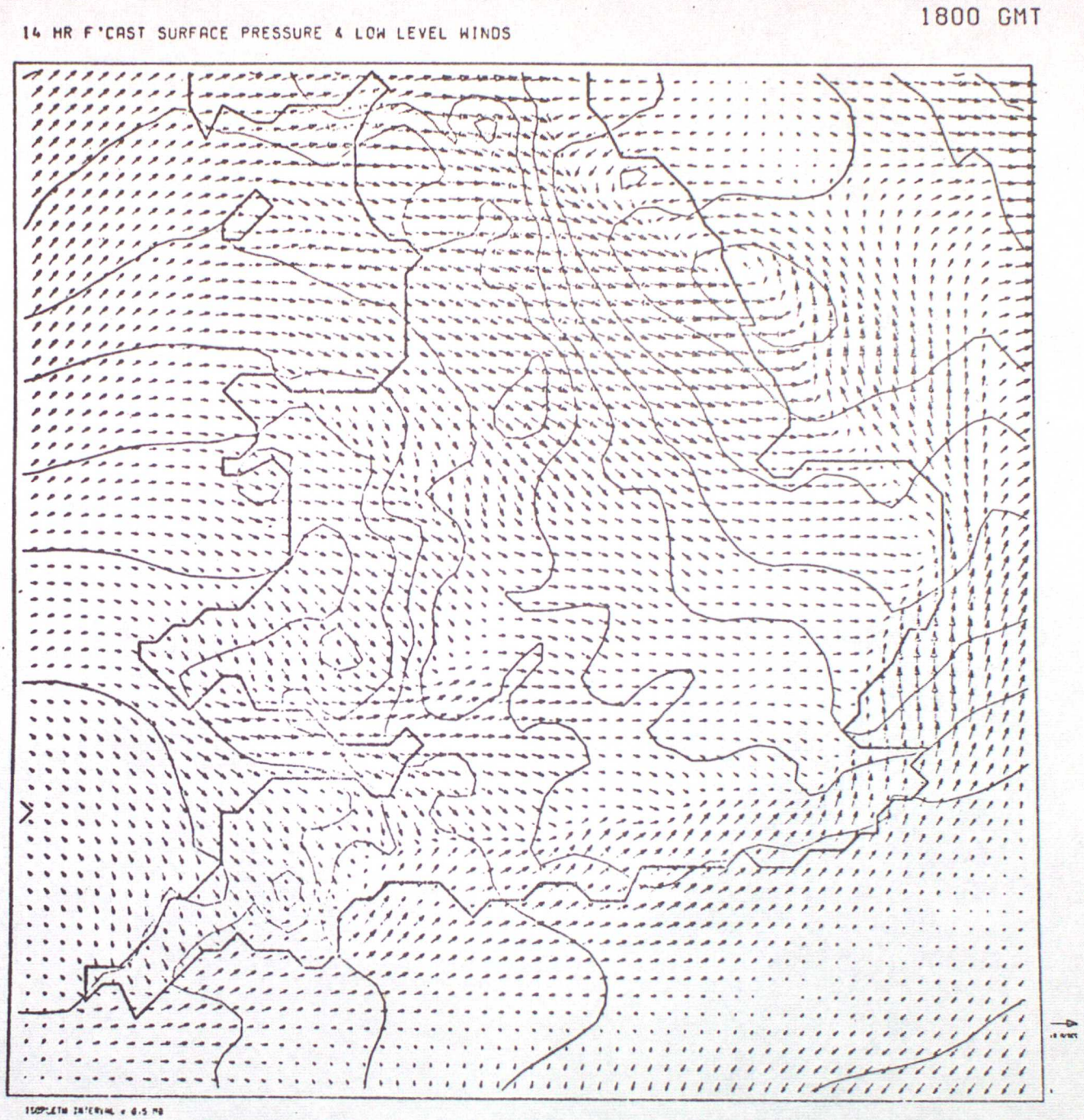

Fig. 4.8

Winds and pressures forecast for 1800 GMT if orography is included in the model. Compare this with Fig. 4.5.

Fig. 4.9

The orographic heights used in the mesoscale model for England and Wales.

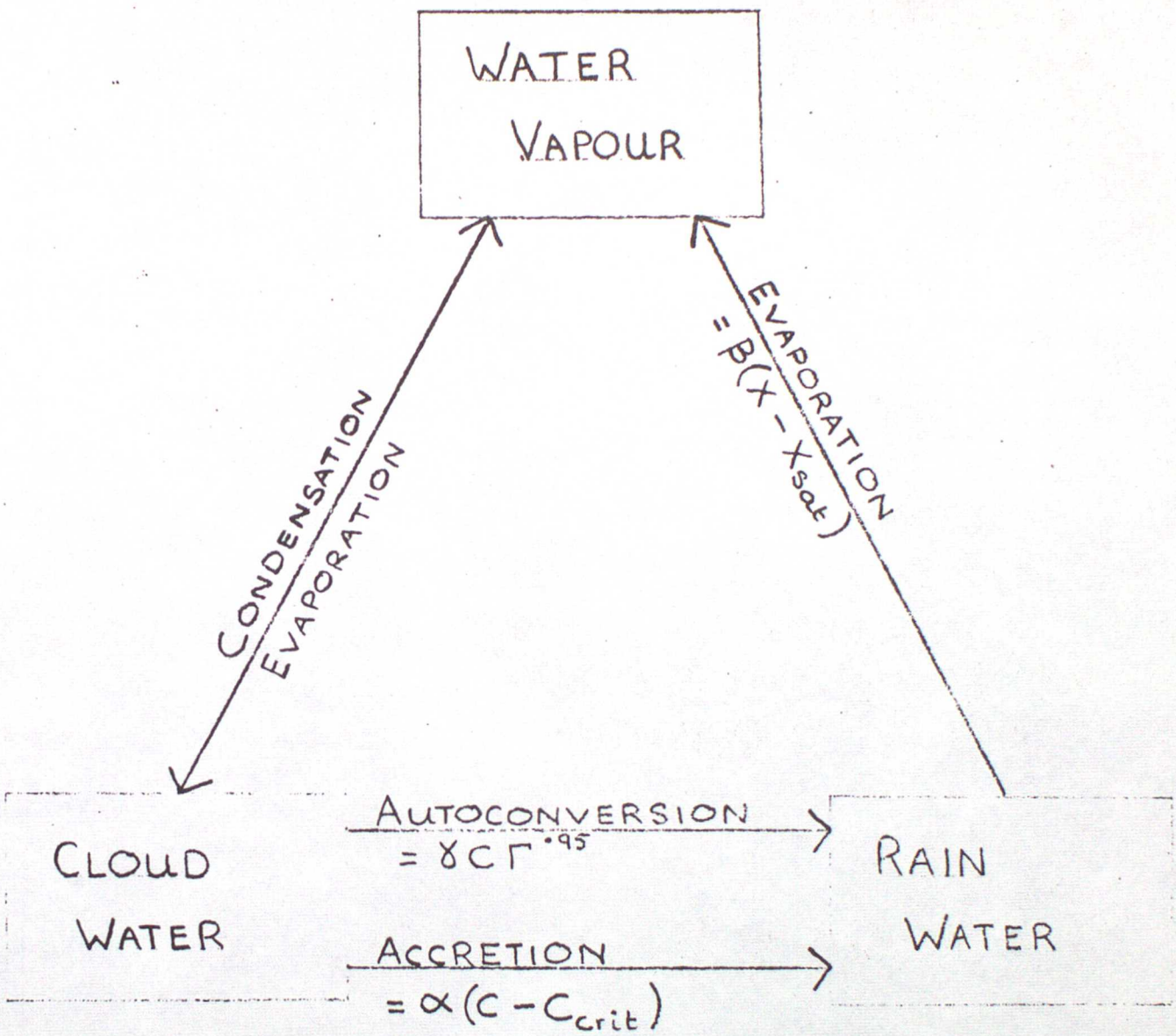

Fig. 5.1

The conversion between the three phases of water included in the cumulus model.

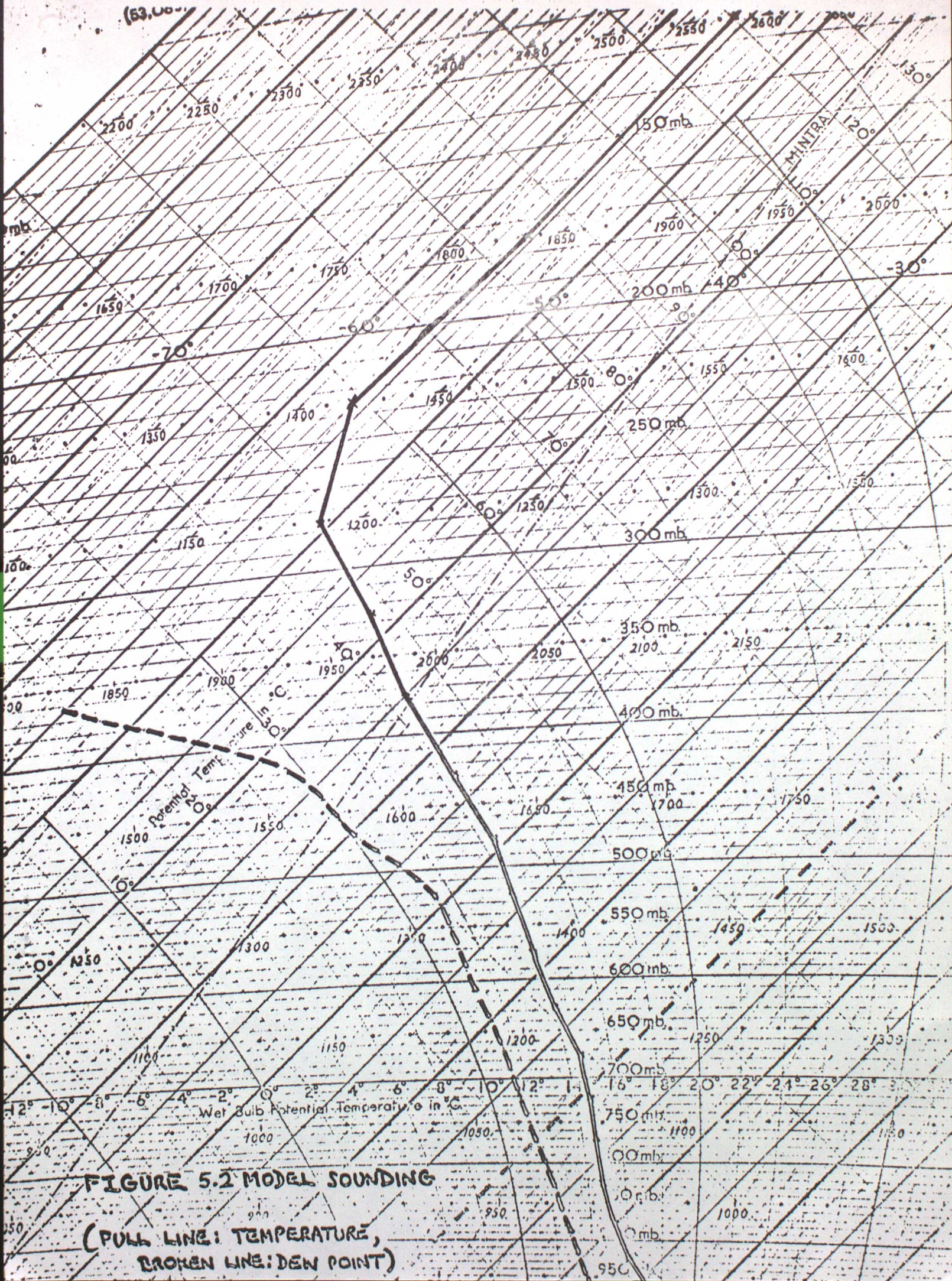

FIGURE 5.2 MODEL SOUNDING

(FULL LINE: TEMPERATURE,
BROKEN LINE: DEW POINT)

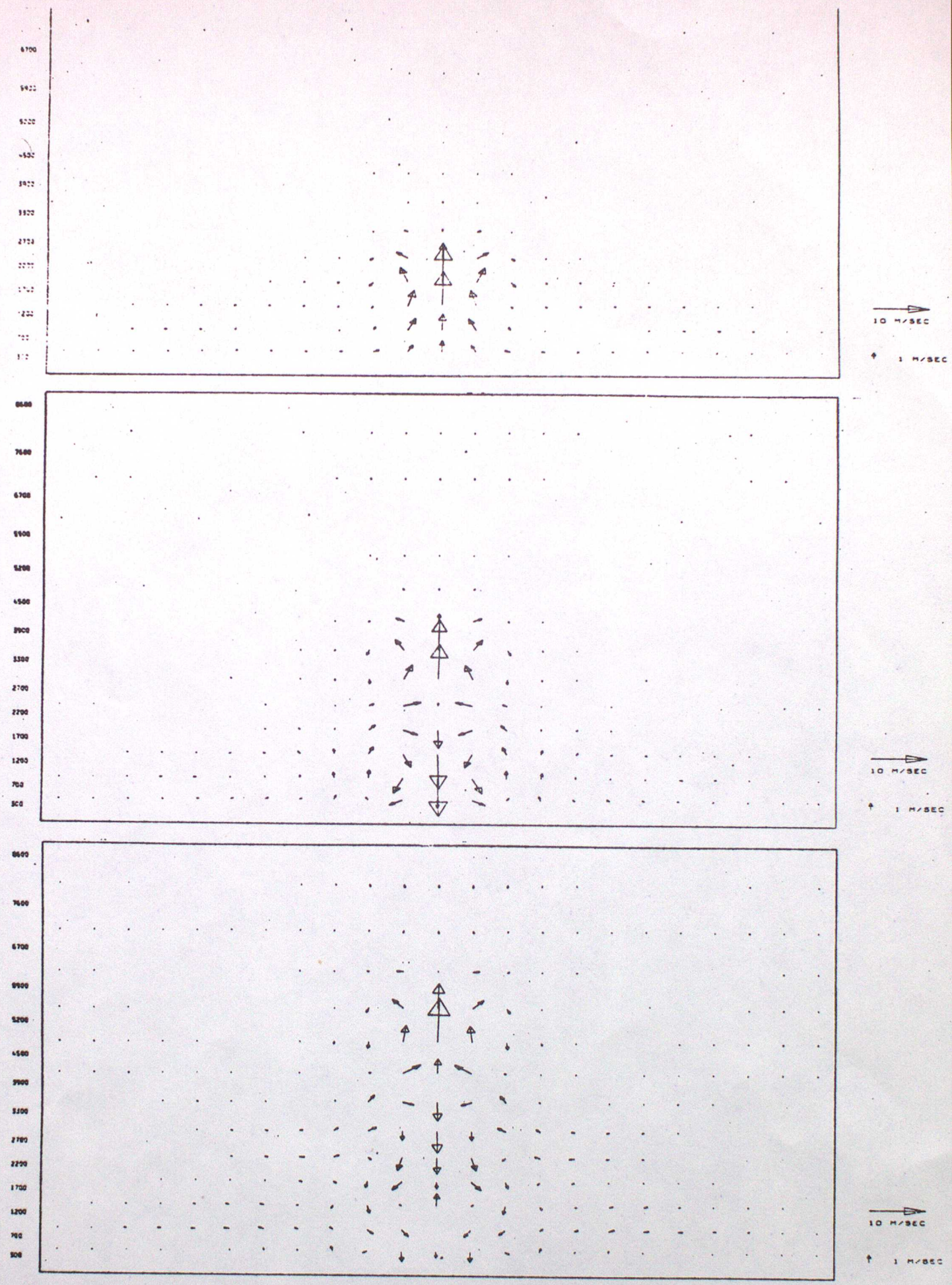

Fig. 5.3

Cross sections through the cloud showing wind vectors at 35mins (top), 45mins (middle) and 55mins (bottom) from the start of the integration.

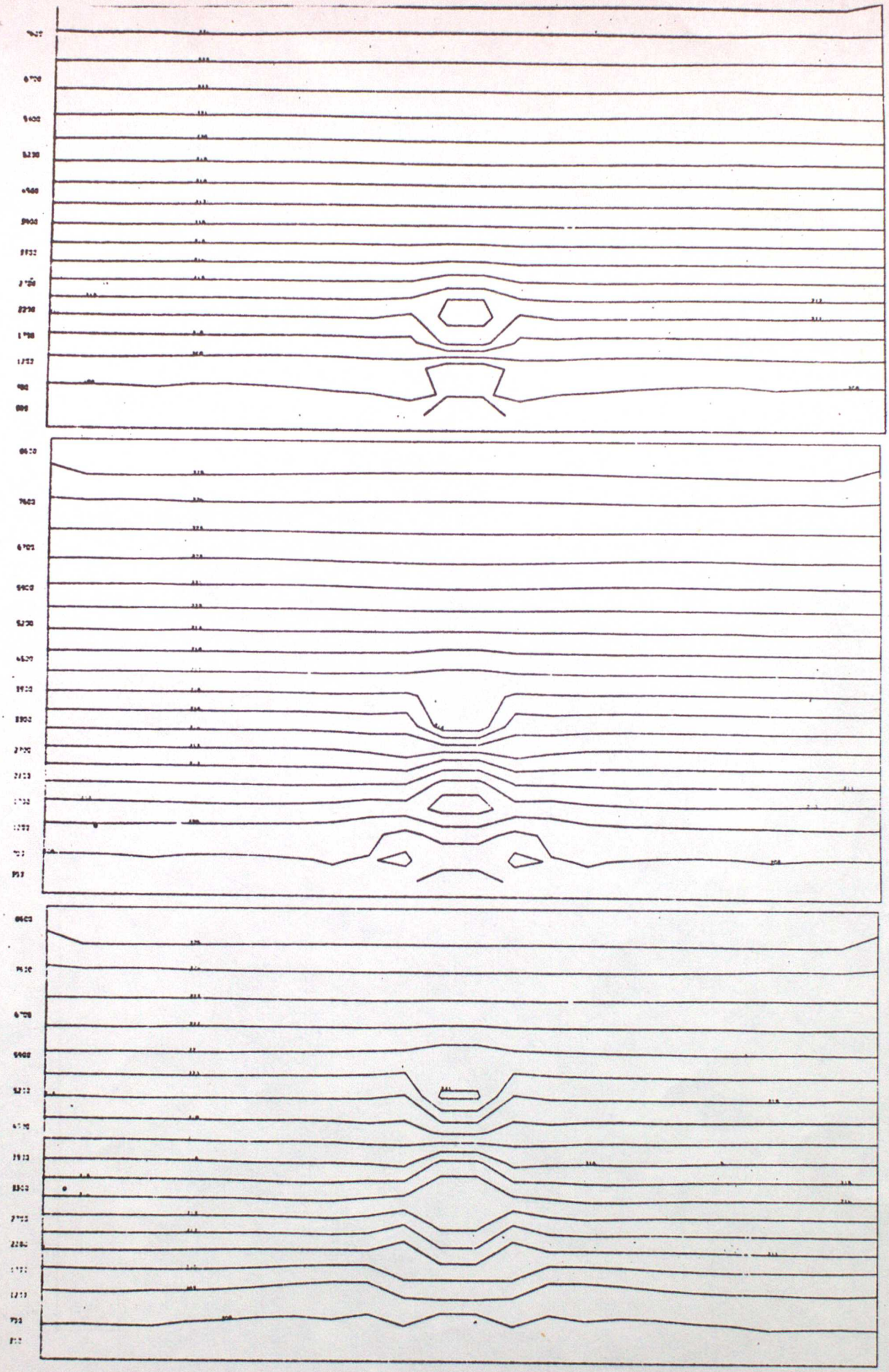

Fig. 5.4

Cross sections through the cloud showing potential temperature (isopleth interval 1K) at 35mins (top), 45mins (middle) and 55mins (bottom) from the start of the integration.

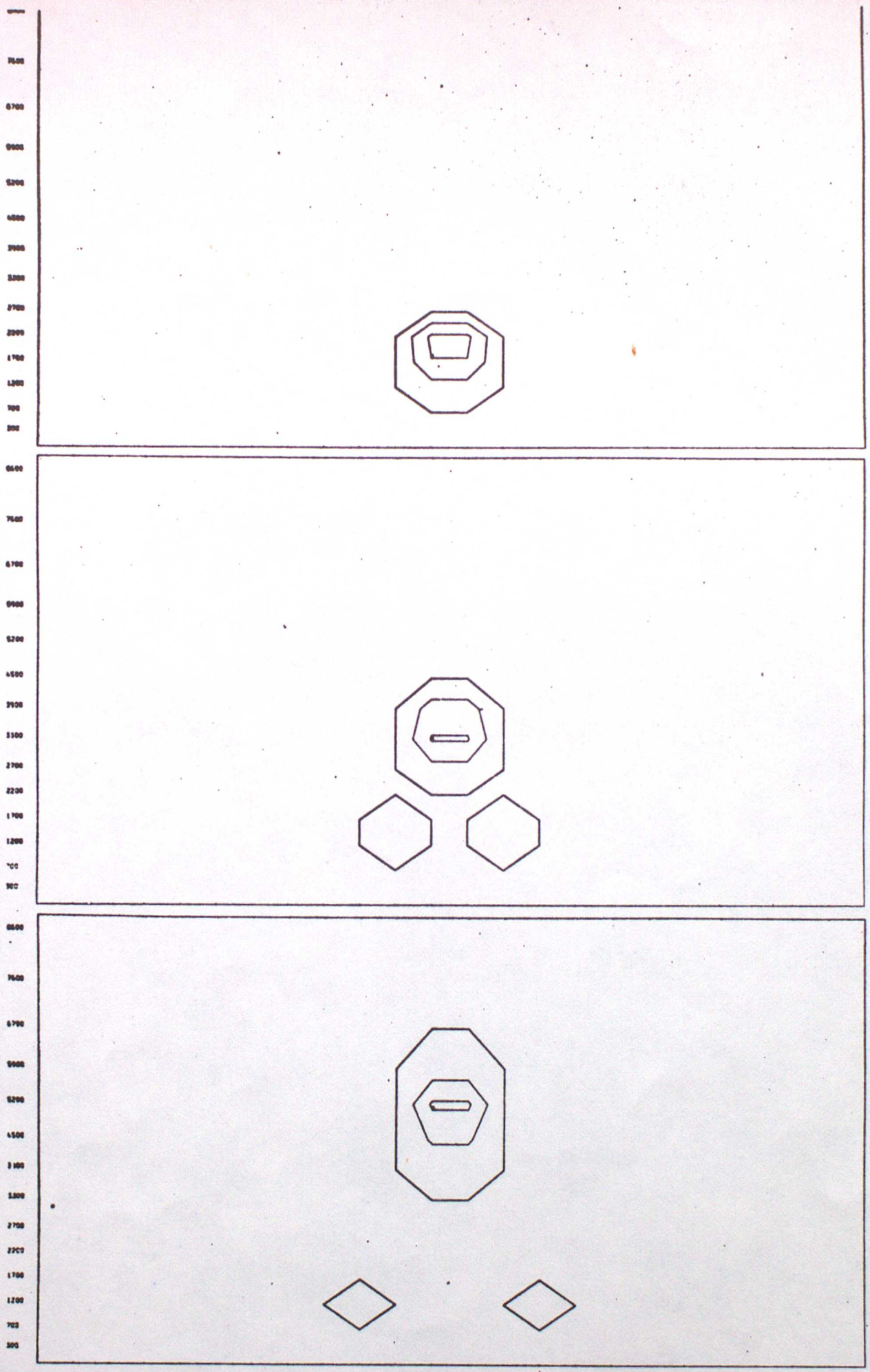

Fig. 5.5

Cross section through the cloud showing cloud water amount (isopleths of 0,1,2etc. gm/kg) at 35mins (top), 45mins (middle) and 55mins (bottom) from the start of the integration.

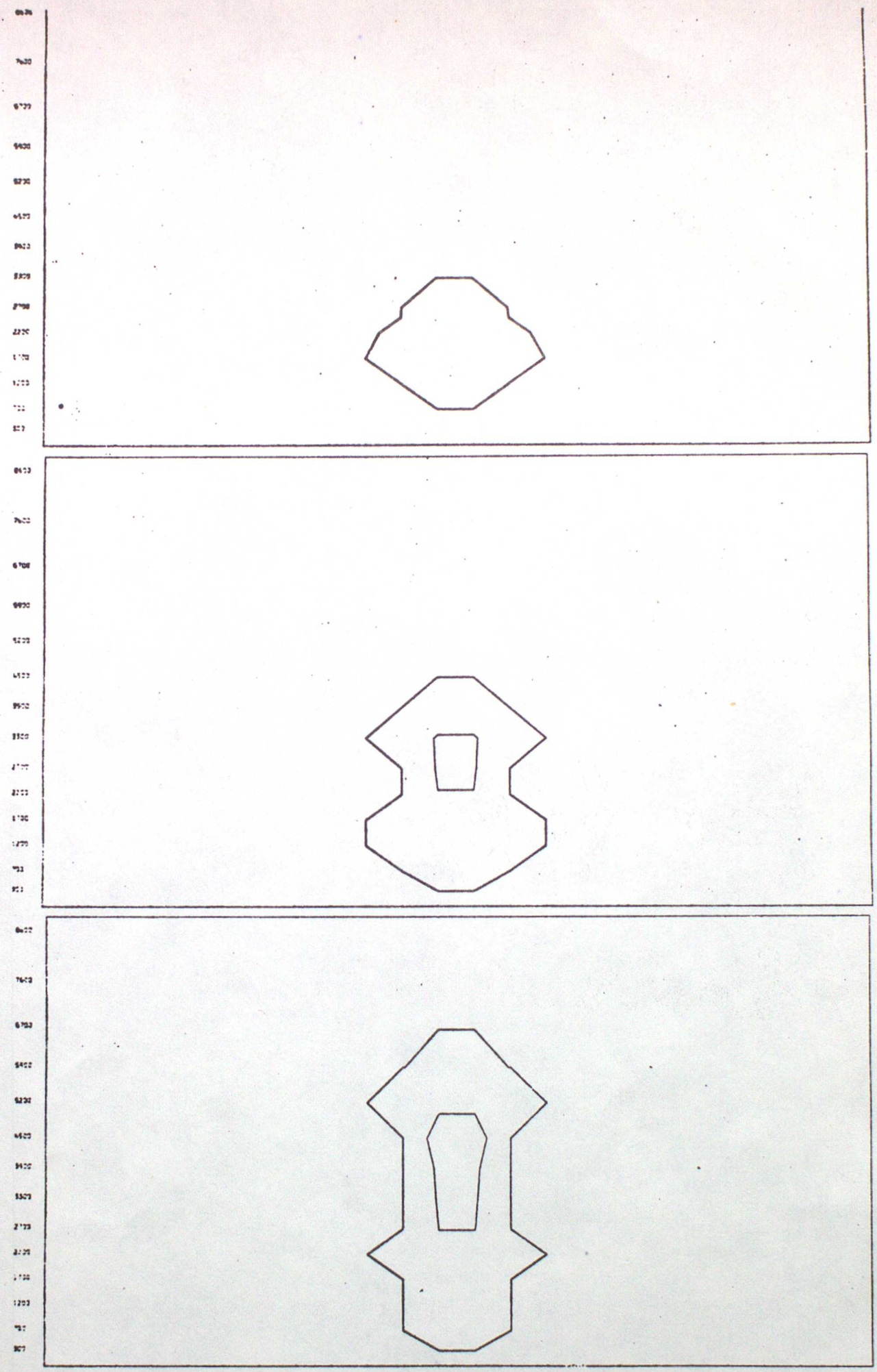

Fig. 5.6

Cross sections through the cloud showing rain water amount (isopleths of 0,1,2etc. gm/kg) at 35mins (top), 45mins (middle) and 55mins (bottom) from the start of the integration.